



pubs.acs.org/estengg Review

# Environmental Materials beyond and below the Nanoscale: Single-Atom Catalysts

Seunghyun Weon, Dahong Huang, Kali Rigby, Chiheng Chu, Xuanhao Wu, and Jae-Hong Kim\*



Cite This: https://dx.doi.org/10.1021/acsestengg.0c00136

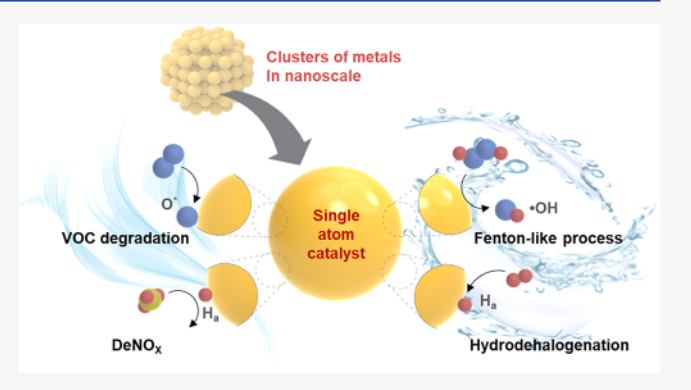


**ACCESS** I

Metrics & More

Article Recommendations

ABSTRACT: Nanotechnology has driven scientific advances in catalytic materials and processes over the past few decades. Unique physicochemical and electronic properties that emerge when materials are engineered from the bulk to the nanoscale have been exploited for a wide range of applications, including environmental remediation such as catalytic pollutant destruction. Recent advances in the catalytic synthesis of fuels and value-added chemicals explore the properties of materials, noble and transition metal catalysts in particular, when they are engineered to be below nanoscale and at the single-atom limit. In addition to the maximized efficiency of atomic utilization due to size reduction, significantly reduced costs and the potential to achieve highly selective catalysis are particularly appealing to the environmental



application of single-atom catalysts, overcoming certain limitations that the field has been unable to address with nanotechnology. This critical review, built upon a comprehensive discussion of fundamental properties, synthesis methods, and application examples, evaluates in depth the opportunities and challenges of single-atom catalysts as new frontier materials for environmental remediation applications beyond nanomaterials.

KEYWORDS: single-atom catalyst, isolated atom, nanomaterial, environmental application, review

# **■ INTRODUCTION**

Nanotechnology has undoubtedly led the scientific advancement of catalytic materials and processes over the past few decades. The most evident advantage that nanomaterials have over bulk materials is their larger surface area and increased number of catalytic sites. In addition, unique physicochemical properties that emerge as materials are engineered from the bulk to the nanoscale have been essential to enable unconventional catalytic reactions. The significant benefits of downsizing materials can be illustrated by gold, a noble metal widely used in the nanoscale. Though gold is chemically inert when in the bulk state, gold nanoparticles exhibit nanoscale phenomena, including surface plasmon resonance and altered electronic structure, which enable distinctive photothermal and catalytic functions. <sup>1–4</sup> This motivates the question of what would happen if the same material were engineered on the subnanoscale. In other words, can the material be engineered to exist as a "single atom", which is the theoretical limit in our endeavor to reduce the size of materials, resulting in improved catalytic performance and allowing functions impossible at the nanoscale? Such catalytic materials are referred to as singleatom catalysts (SACs), a term first used by Qiao et al. to describe isolated single Pt atoms immobilized on the surface of iron oxide for CO oxidation catalysis.5

SACs represent the forefront of catalysis research today in both theoretical and experimental studies. Since each atom in SACs is able to participate in catalytic reactions instead of being buried and inevitability wasted inside nanoparticles, the atomic efficiency reaches the theoretical maximum of 100%.6,7 SACs are named as such due to the separation of active metals from one another, i.e., the lack of metal-metal bonding. Atomically dispersed noble or transition metals possessing extremely high surface energy are realized by strong interactions between metals and support materials (e.g., metal oxide, graphene, metal carbide, carbon nitride, etc.), which prevent the aggregation of individual metal atoms.<sup>8,9</sup> Due to this strong interaction between single metal atoms and the support material, a dynamic charge transfer can occur, affecting the way metals participate in catalysis. 10 The unique electronic structure within the unsaturated coordination of the single atom is also distinct from its metallic nanocluster

Received: September 10, 2020 Revised: September 14, 2020 Accepted: September 14, 2020



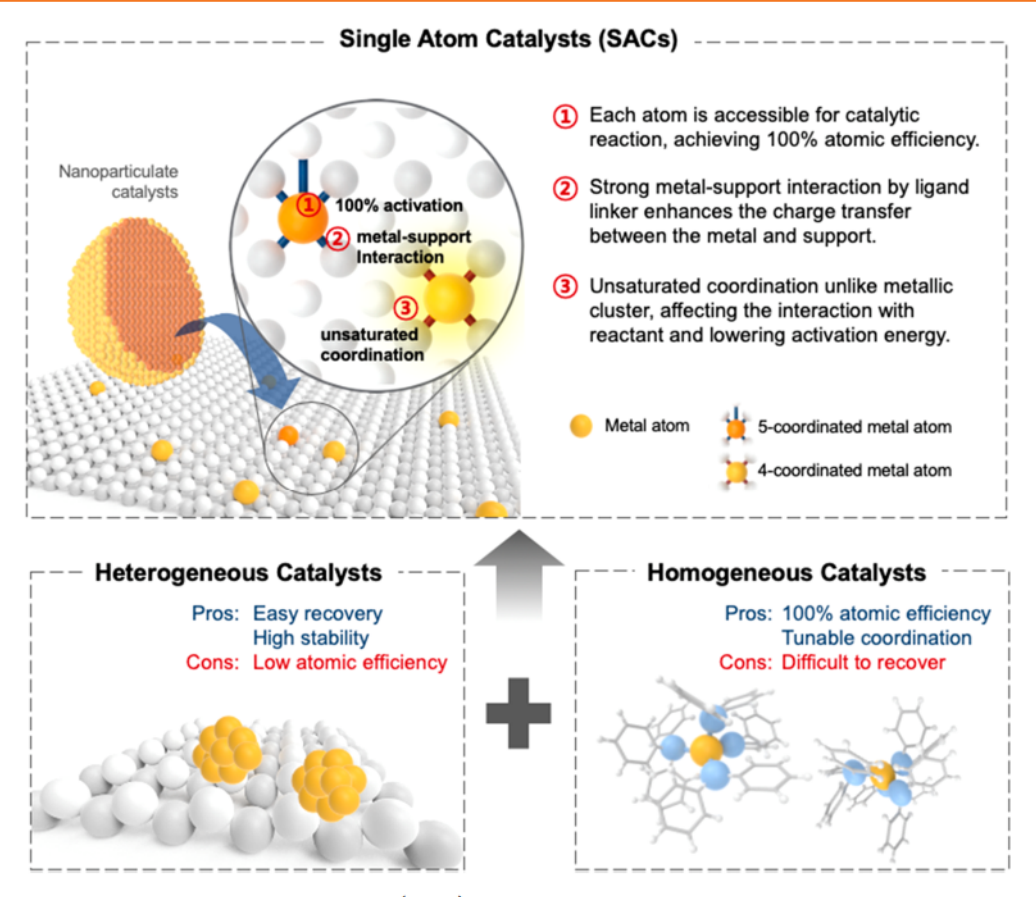


**Figure 1.** Definition and properties of single-atom catalysts (SACs). The yellow spheres represent noble or transition metal atoms. The collection of white spheres represents the support material. The blue and red lines between yellow and white spheres represent coordination bonding between the metal and support material.

counterparts and has been shown to confer unprecedented catalytic properties. Alternatively, single metal atoms can be anchored onto another metal host in a configuration referred to as a single-atom alloy (SAA) to exhibit unique bimetallic functionality. The rapid emergence of SAC applications in various fields, including chemical synthesis,  $^{13,14}$  CO $_2$  reduction, and hydrogen evolution, highlights their vast potential.

While the benefits of nanomaterials have facilitated their successful implementation into multiple fields, 17,18 their adoption to environmental applications has been slower, partly due to a relatively high material cost barrier. 19 Therefore, the minimal use of noble metals and the maximized atomic efficiency of a single atom are particularly appealing for environmental applications. Palladium catalysts, for example, are well-known for their ability to reductively remove a number of priority drinking water contaminants. 20 In the form of nanoparticles with a diameter of 5 nm, 78.6% of Pd atoms are buried and inactive, while all Pd atoms in the form of SACs are available for the reaction and highly active. The material cost of Pd SACs (one atom dispersed per 10 nm<sup>2</sup> support, ~1 wt % loading) to cover a 1 m<sup>2</sup> surface would be 220 times less expensive than Pd nanoparticles (5 nm in diameter, typical for environmental nanomaterials<sup>21-23</sup>).

Thus, far, SAC research has primarily focused on fuel and chemical syntheses. Many recent studies in these fields, well summarized in previous reviews, 12,24-28 claim that SACs possess better catalytic efficiency and selectivity than their larger counterparts. SACs can likewise be applied to environ-

mental fields, potentially opening a largely untapped opportunity and effortlessly incorporating catalysis into solving various challenging environmental problems. In this critical review, we first introduce the properties, synthetic procedures, and characterization methods that are essential for researchers who wish to explore SAC materials for environmental applications. We further discuss a few environmental remediation scenarios that can benefit from SACs, with a critical assessment of their challenges and research needs.

## ■ PROPERTIES OF SINGLE-ATOM CATALYSTS

SACs exhibit distinct advantages of both homogeneous and heterogeneous catalysts (Figure 1).<sup>29</sup> Homogeneous catalysts in the aqueous phase, which are often in the form of an organometallic complex, offer fast reaction kinetics and maximized metal utilization efficiencies. Their most compelling property is tunable metal-ligand interactions, providing a welldefined coordination environment for selective catalytic processes. However, such catalysts in general present low economic value and limited applications due to (i) the difficulty of catalyst separation and recycling after use and (ii) the structural instability of the organic ligands, especially in pollutant destruction schemes. On the other hand, heterogeneous catalysts, including nanoparticulate catalysts, can be relatively easily recovered and regenerated, which is appealing for practical applications.<sup>30</sup> However, their atomic efficiency is much lower and kinetics often slower than their homogeneous counterparts due to their much lower surface atom ratio.

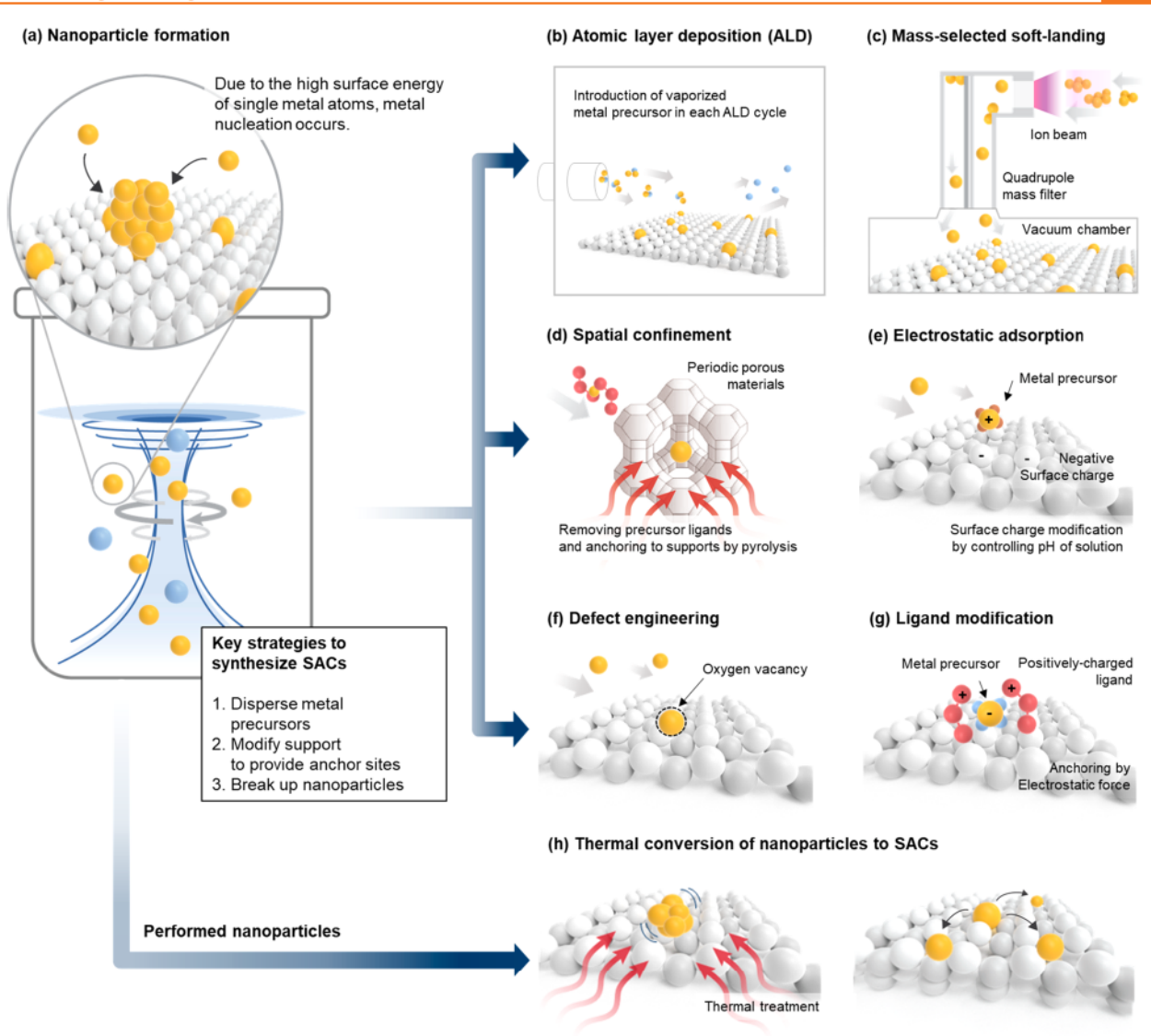


Figure 2. Schematic illustrations of (a) representative nanoparticulate catalyst synthesis method and (b)—(h) various SAC synthetic methods. In SAC synthesis, dispersion of metal precursors across support surface can be achieved by (b) atomic layer deposition, (c) mass-selected soft-landing, and (d) spatial confinement using periodic porous materials. (e) Electrostatic attraction can bring SAC precursors to support surface, but anchoring sites such as (f) defects and (g) surface ligands are necessary to achieve high SAC loading to prevent metal cluster formation. In an alternative approach not involving precursors, (h) thermal treatment can transform preformed nanoparticles to SACs.

SACs resemble heterogeneous catalysts since they are immobilized on supports that can be separated for reuse. SACs, at the same time, resemble homogeneous catalysts as the strong metal-support interactions yield electronic properties similar to those in organometallic complexes. The surface free energy of metals increases when they exist as single atoms, leading to the aggregation tendency of atomically dispersed atoms during synthesis and use.31 Strong binding to adjacent atoms of the support material not only prevents metal migration and aggregation but also makes SACs behave like mononuclear homogeneous catalysts.<sup>32</sup> It is therefore possible to realize homogeneous redox catalytic reactions in a heterogeneous fashion, as the strong interaction between single metal atoms and a conductive support efficiently mediates charge transfer. <sup>31,33</sup> For example, single-atom Co bound to adjacent N atoms of N-doped graphene in a CoN4 structure (four nitrogen-coordinated Co atom) was shown to efficiently catalyze a Fenton-like reaction through charge transfer.<sup>34</sup> In addition, the absence of metal ensembles can

produce unexpected selective catalytic reactions by inhibiting reaction pathways occurring at identical metal atoms coordinated with the active metal site. For example, atomically dispersed Pd on an Au–Pd nanoalloy enhanced  $\rm H_2O_2$  production, while two adjacent Pd atoms on Pd nanoparticles favored the simultaneous reduction of two oxygen atoms, producing  $\rm H_2O$  molecules. <sup>35</sup>

The capability to tune the coordination environment of a single-atom catalytic center like homogeneous catalysts makes SACs distinctively advantageous over other heterogeneous catalysts. The coordination environment can be manipulated by altering the type of coordinating atoms in the support. For example, single-atom Pt showed higher selectivity toward electrochemical H<sub>2</sub>O<sub>2</sub> production when loaded onto TiC compared to TiN. Due to the strong affinity of oxygen molecules for the N atoms coordinated to Pt, the O<sub>2</sub> dissociation reaction occurred preferentially (i.e., instead of O<sub>2</sub> reduction), resulting in the decreased H<sub>2</sub>O<sub>2</sub> production efficiency of single-atom-Pt-loaded TiN.<sup>36</sup> In addition to atoms

at the first coordination shell of the catalyst atom, vicinal cations in the support material that form the second coordination shell can affect catalytic performance as well.<sup>37</sup> For instance, single-atom Pt on a CeO<sub>2</sub> support exhibited high activity for CO oxidation even at low temperature,<sup>38</sup> while the same single-atom Pt on a SiO<sub>2</sub> support was ineffective and even worse than its nanoparticle counterparts.<sup>39</sup> It was found that CO oxidation on Pt<sub>1</sub>/CeO<sub>2</sub> occurred through concerted adsorption of CO on Pt<sub>1</sub> and O<sub>2</sub> dissociation/activation on reducible Ce atoms.<sup>40,41</sup> In contrast, CO oxidation was retarded when inert SiO<sub>2</sub> was used as a support due to competitive adsorption between CO and O<sub>2</sub> on single-atom Pt.<sup>42</sup>

The catalytic performances of metals can also be altered by manipulating the coordination number. 34,43 For instance, single-atom Pt exhibited improved activity for the hydrogenation of 3-nitrostyrene as Pt-O coordination decreased from 3.8 to 1.8. Decreased coordination to O results in lower Pt oxidation states, significantly increasing hydrogenation activity without the loss of chemoselectivity.44 As another example, single-atom Ni in Ni-N2-C achieved higher activity for CO2 electrochemical reduction over Ni in Ni-N3-C and Ni-N<sub>4</sub>-C by facilitating the formation of a COOH\* intermediate.<sup>45</sup> Although unsaturated coordination sites of a single-atom center have been generally recognized as the critical advantage of SACs, lowering the coordination number does not necessarily lead to an elevated catalytic performance toward the target reaction. 46,47 An optimal coordination environment may be obtained at a higher coordination number, which could enhance the adsorption of a reactant or desorption of a product. For example, Fe-N<sub>5</sub> displayed a higher electrocatalytic performance for CO2 reduction than Fe-N<sub>4</sub> due to promoted CO desorption.<sup>48</sup> The relationship between the coordination environment of SACs, determined by both the species of coordinating atoms and the coordination number, and their catalytic performance varies depending on the types of materials and target reactions. Understanding these relationships at the atomic level remains a fundamental challenge and presents significant research needs for various catalytic reactions relevant to environmental remediations.

# SYNTHESIS METHODS

The starting materials and procedures for synthesizing SACs are mostly similar to those for nanoparticulate catalysts. Loading single-atom metals onto a substrate surface at very low concentrations is relatively easy when the precursor concentration is very low. But these sparsely doped materials are not preferred due to low catalytic efficiency. In contrast, synthesizing SACs at high loading remains a challenging task. When the concentration of metal precursor increases, metal atoms tend to coalesce and form clusters due to high surface free energy, which eventually leads to nanoparticle formation (Figure 2a). The key to synthesize SACs is how to ensure the atomic dispersion of metal precursors during synthesis.

Early SAC studies relied on rather complicated synthesis techniques, such as atomic layer deposition (ALD)<sup>49–51</sup> and mass-selected soft-landing.<sup>52–54</sup> These methods employ vaporized metal precursors to minimize interactions among precursors and prevent interference with impurities. In a typical ALD process (Figure 2b), the metal precursors carried by an inert gas are first chemisorbed to the support surface. Metal atoms are then coordinated to the active sites through a

reaction with the second precursor that is subsequently introduced as a vapor, completing a single ALD cycle. The self-limiting nature of precursor reactions prevents metal loading beyond a single atomic layer in each ALD cycle. The SAC loading is controlled by the number of ALD cycles, and excessive ALD cycles can lead to the formation of nanoclusters. Mass-selected soft-landing (Figure 2c) involves guiding positively charged metal ions from vacuum chambers toward the substrate through a quadrupole mass filter based on mass to charge ratio. Though such methods are advantageous for the precise synthesis of SACs, both require sophisticated instruments and suffer from low material yield. Therefore, they are generally considered unsuitable for large scale production. 55

Wet chemical methods, such as coprecipitation and impregnation, are inexpensive and easy to implement without requiring specialized instruments. 56-58 However, since the precursor metals are brought to the support surface in a less controlled manner compared to the aforementioned gas-phase approaches, it is critical to provide spatially confined anchoring sites that can host no more than a single metal atom. The spatial confinement of single-atom metals within molecular/ atomic-scale cages has been used as an effective approach to prevent the migration and aggregation of metal precursors. Periodic porous materials, such as metal organic frameworks (MOFs), 59-61 covalent organic frameworks (COFs), 62 and zeolites, 63,64 allow for the spatial and atomic distribution of metal species to achieve relatively high SAC loading (Figure 2d). For example, single-atom Pt and Ir with mass loadings up to 2.54% and 1.05%, respectively, were synthesized on a zirconium porphyrin-based MOF as a spatially confining template. 65 However, this approach is limited by the availability of specific porous substrates and the difficulty of completely removing unreacted metal precursor ligands during post treatment.

Alternative approaches to extend wet chemical syntheses to a wider range of support materials have been extensively pursued through modifying surface properties. By controlling the pH of aqueous solutions containing both supports and metal precursors, SACs can be synthesized through electrostatic adsorption between supports and metal ions. For example, a single Pt atom per 5 nm diameter TiO<sub>2</sub> particle was achieved by electrostatic adsorption between a surface oxygen anion (O<sup>-</sup>) and platinum tetraammine ([(NH<sub>3</sub>)<sub>4</sub>Pt]<sup>2+</sup>) at pH 12. Here was achieved by electrostatic adsorption between a surface oxygen anion (O<sup>-</sup>) and platinum tetraammine ([(NH<sub>3</sub>)<sub>4</sub>Pt]<sup>2+</sup>) at pH 12.

However, in order to achieve high SAC loading, the availability of specific anchoring sites that provide strong binding for metal atoms is essential. 69,70 Without such sites, metal atoms on the substrate tend to migrate and form aggregates to reduce their surface energy, much like how nanoparticles form during similar wet chemical syntheses. Some materials have anchoring sites that can host single atoms in their inherent structures. For example, the void center of C<sub>3</sub>N<sub>4</sub> nanosheets can anchor a Co single atom by forming a stable coordination with pyridinic N atoms in the surrounding heptazine units of C<sub>3</sub>N<sub>4</sub>.<sup>72</sup> For crystalline substrates, defects such as unsaturated sites and vacancies can be introduced as such anchoring sites (Figure 2f). For example, Au can be anchored onto TiO2 nanosheets with abundant oxygen vacancies on its surface by forming a Ti-Au-Ti structure, while Au tends to form nanoparticles on the surface of pristine TiO<sub>2</sub>. As another example, single Rh atoms can be trapped to Mo defect sites, a cationic vacancy, on defect-rich  $MoS_4$  nanosheets to form a  $Rh{-}S_4$  structure.

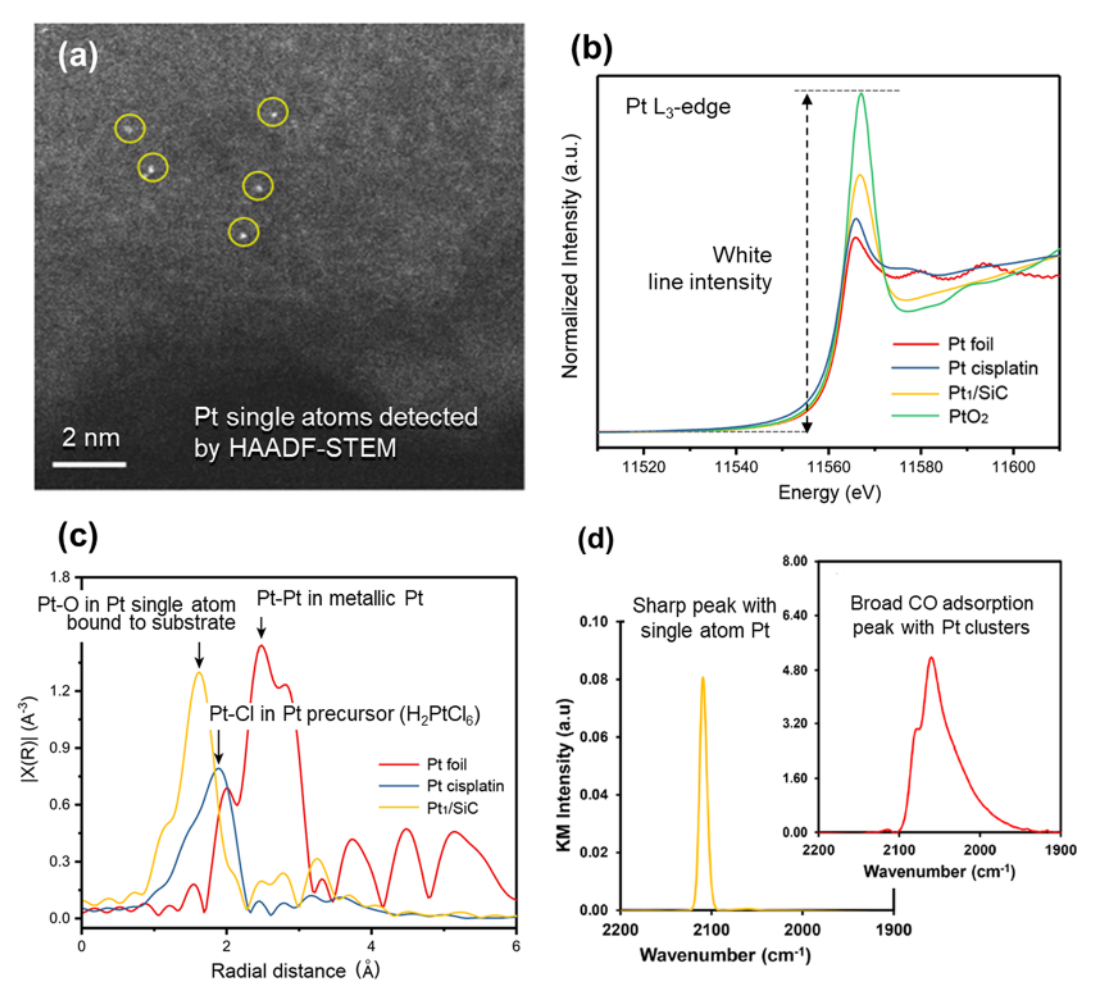


Figure 3. Characterizations of Pt SACs (Pt<sub>1</sub>). (a) HAADF-STEM image that shows atomically dispersed Pt single atoms (highlighted by yellow circles) on N-doped carbon. Reprinted in part with permission from He et al. <sup>86</sup> Copyright 2019 Springer Nature. (b) Normalized XANES measurements at the Pt L<sub>3</sub>-edge (11.5637 keV, ionization energy of 2p (j = 3/2) electron of Pt) of Pt<sub>1</sub>/SiC, Pt cisplatin, Pt foil and PtO<sub>2</sub>. (c) Fourier transform of the  $k^3$ -weighted EXAFS (where k is the wavenumber of the photoelectron, and EXAFS often weighted by  $k^2$  or  $k^3$  to amplify oscillation signals) of Pt<sub>1</sub>/SiC, Pt foil, and Pt cisplatin. Reproduced from Huang et al., <sup>71</sup> with permission. Copyright 2018 American Chemical Society. (d) IR spectra of CO adsorption at saturation coverage and room temperature to atomically dispersed Pt on TiO<sub>2</sub> and Pt clusters on TiO<sub>2</sub>. Reproduced from DeRita et al., <sup>68</sup> with permission. Copyright 2017 American Chemical Society.

Functionalization of supports with surface ligands (Figure 2g) is an alternative approach that overcomes the difficulty of uniformly introducing defect sites. For example, a relatively high loading of Pd SAC ( $\sim$ 1.5 wt %) was achieved on TiO<sub>2</sub> coated with ethylene glycol, as more than one oxygen atom of ethylene glycol coordinates with a Pd single atom; in contrast, Pd nanoparticles formed on ligand-free TiO<sub>2</sub>. To Up to 1.6 wt % Pt was loaded as single atoms on a SiC substrate modified with (3-aminopropyl)trimethoxysilane. The negatively charged Pt precursor (PtCl<sub>6</sub><sup>2-</sup>) arranged to the positively charged ammonium group on SiC via electrostatic attraction. Subsequent photoreduction formed Pt—O bonds that provide strong anchors to Pt SACs.

A challenge remains in ensuring the stability of the metal—substrate bond over long-term use under harsh conditions. SACs may still aggregate to form nanoparticles, especially under high-temperature applications. A novel strategy to obtain thermally stable SACs has been explored on the basis of a top-down route from metal nanoparticles by thermal treatment (Figure 2h). 74,75 Wei et al. reported an unexpected phenomenon where noble metal nanoparticles (Pd, Pt, and Au) were transformed to thermally stable SACs above 900 °C

in an inert atmosphere.<sup>76</sup> High-temperature conversion of nanoparticles to SACs yielded thermodynamically stable metal—N<sub>4</sub> structures when mobile metal atoms were immobilized in defects of nitrogen-doped carbon. Using this method, SACs overcome the drawback of high-temperature aggregation, a common challenge in industrial applications.

# ■ CHARACTERIZATION TECHNIQUES

After the invention of scanning probe microscopy and related techniques in the 1980s that can image structures on the nanoscale, the door to the nanoworld was pushed open. 77,78 Similarly, the development of high-end instruments has been key for advances in SAC science. The techniques that are used for nanoparticle characterization, such as transmission electron microscopy (TEM), X-ray powder diffraction (XRD), X-ray photoelectron spectroscopy (XPS), atomic force microscopy (AFM), and ultraviolet—visible spectroscopy (UV—vis), cannot prove the presence of SACs, although they still remain useful to analyze the substrates that host single atoms. Some of these analyses can be used as a negative control. For example, the lack of nanoparticles in TEM images may indicate that the metals on the substrate can be on the atomic scale. However, it

does not exclude the possibility that metals can also exist as clusters whose size is smaller than the resolution of the instrument.

In order to present undeniable evidence for the formation of SACs, a suite of characterization techniques must be utilized. A visual confirmation of single-atom configuration can be obtained by high-angle annular dark-field scanning transmission electron microscopy (HAADF-STEM). Conventional TEM techniques do not provide sufficient contrast for single atoms to be seen, even when high-resolution TEM or brightfield TEM is employed.<sup>79</sup> In HAADF-STEM, an electron beam is focused and raster-scanned over the sample, and the transmitted electrons that are scattered at high angles are collected using an annular detector. Incoherent Rutherford scattering that occurs through the interaction between the incident electrons and the nuclei mainly contributes to the high-angle scattering.<sup>79-81</sup> Since greater electrostatic interactions between the nucleus and incident electrons cause electrons to be scattered, the image intensity becomes approximately proportional to the square of the atomic number. 82,83 This makes heavier metal catalysts appear much brighter than the lighter atoms that constitute the support, enabling compositional imaging of metals at atomic resolution. Aberration correction of the probe in STEM can further enhance the image contrast and resolution by focusing the electron beam below an Ångstrom, thereby increasing the interaction with the single atom. The first STEM imaging of single atoms was performed in 1970, when single uranium atoms were viewed on a carbon film.<sup>84</sup> Since then, many more single-atom dispersions have been characterized using STEMbased techniques, with a great push forward arising from platinum-group metals.85 Figure 3a is a sample HAADF-STEM image of Pt SACs loaded on N-doped carbon, where atomically dispersed Pt atoms (highlighted by yellow circles) were observed over the support material with no obvious Pt nanoparticles or clusters.<sup>86</sup> Since HAADF-STEM images provide only visual confirmation, not chemical information such as valency or coordination, it must be used in conjunction with other techniques.

X-ray absorption spectroscopy (XAS) yields valuable information about the SAC's oxidation state and coordination environment. This technique, which requires a synchrotron source, involves irradiating X-rays of tunable incident energies to excite core electrons of the sample. XPS, a similar and common technique, generates an electron beam energy as high as 5000 eV with a top-notch Cr K $\alpha$  source, but this is far from enough energy to photoeject the core electrons of metals (e.g., excitation energy of 2p (j = 3/2) electron of Pt is 11563.7 eV). Additionally, the synchrotron source provides a spectral brilliance unmatched by standard XPS, which is made tunable via an X-ray monochromator. X-ray absorption near-edge structure (XANES) and extended X-ray absorption fine structure (EXAFS) are typical analyses performed with the data from XAS measurements. XANES provides information on the electronic structure of the absorbing atom, and EXAFS provides information on the number and bonding distances of the atoms surrounding the absorbing atom.

XANES comprises the spectral components near the absorption edge, a feature produced by the dramatic increase in the absorption of X-rays at the absorption edge energy position (Figure 3b). This sharp peak at the top of the edge is called the white line, a name arising from the appearance of X-ray absorption data on photographic plates. XANES scans 30—

50 eV above the atomic core level ionization energy, at which point a photoelectron is emitted with its wavelength larger than the interatomic distance between the specific atom and its nearest neighbors. 83,87 The wave function of a photoelectron can be affected by multiple scattering events involving neighboring atoms. Since the edge maxima of white line intensity shifts to higher energies as oxidation state increases (i.e., the binding energy increases with oxidation state), XANES can be used to determine the valency of an atom by comparing it to those of reference materials such as metal oxides and zerovalent metals. The white line also provides complementary information on the oxidation state because oxidation increases the density of vacant states on the absorbing atom and therefore increases the white line intensity. For example, XANES spectra of Pt<sub>1</sub>/SiC suggest that the oxidation state of Pt in Pt<sub>1</sub>/SiC is between 2+ and 4+, as the white line of Pt<sub>1</sub>/SiC lies between that of Pt cisplatin (Pt<sup>2+</sup>) and PtO2 (Pt4+).71 This is especially informative for SACs wherein the metal-support interactions often produce single atoms with partially charged oxidation states.

The EXAFS spectra account for the oscillatory part of the absorption above the edge and include features caused by the influence of surrounding atoms on photoejected electrons. The photoelectrons produced from excitation by the incident X-ray are scattered by the cores of surrounding atoms. 88 The original photoejected electron and the scattered photoelectron's wave functions undergo quantum interference, causing oscillations in the absorption spectrum at energies above the absorption edge. The intensity of the oscillations in the absorption spectrum decreases at higher energies above the edge, i.e., further removed from edge resonance. The intensity and position of the oscillations depend on the distance between the absorber and scattering atoms, as well as the phase shifts of the wave functions that occur from interactions with the absorber and scattering atoms. The EXAFS signal, which is the absorption spectrum beyond the XANES region, normalized per absorber atom, can be used to assess information about the local coordination environment of the atom of interest. The frequencies contained in the EXAFS signal depend on the distance between the metal atom and its neighboring atoms. A Fourier transform of the EXAFS spectrum produces a photoelectron scattering profile as a function of radial distance from the metal atom. In an example shown in Figure 3c, each noticeable signal corresponds to the different types of neighbors and bonding configurations around the absorbing atom, where Pt-Cl, Pt-O, and Pt-Pt coordination show different peak positions.

Both the XANES and EXAFS spectra are used to verify the absence of metallic bonds, which is critical to exclude the possibility of cluster or nanoparticle formation. This is generally more obvious in the EXAFS spectrum because scattering increases with atomic number. Therefore, a heavy metal scatterer such as Pt will lead to a greater scattering intensity than a light element like C or O (assuming the same absorber atom such as Pt). If only isolated Pt atoms exist, there will be no Pt—Pt scattering. Thus, EXAFS provides an on/off signal for the absence/presence of clusters, while the XANES may only show a change in shape of the signal.

Infrared (IR) spectroscopy is another technique used to characterize single-atom catalysts, verify atomic dispersion, and indicate the lack of clusters or nanoparticles. Gaseous CO is commonly used as a probe molecule, as it interacts differently with isolated metals, metal clusters, and nanoparticles, and

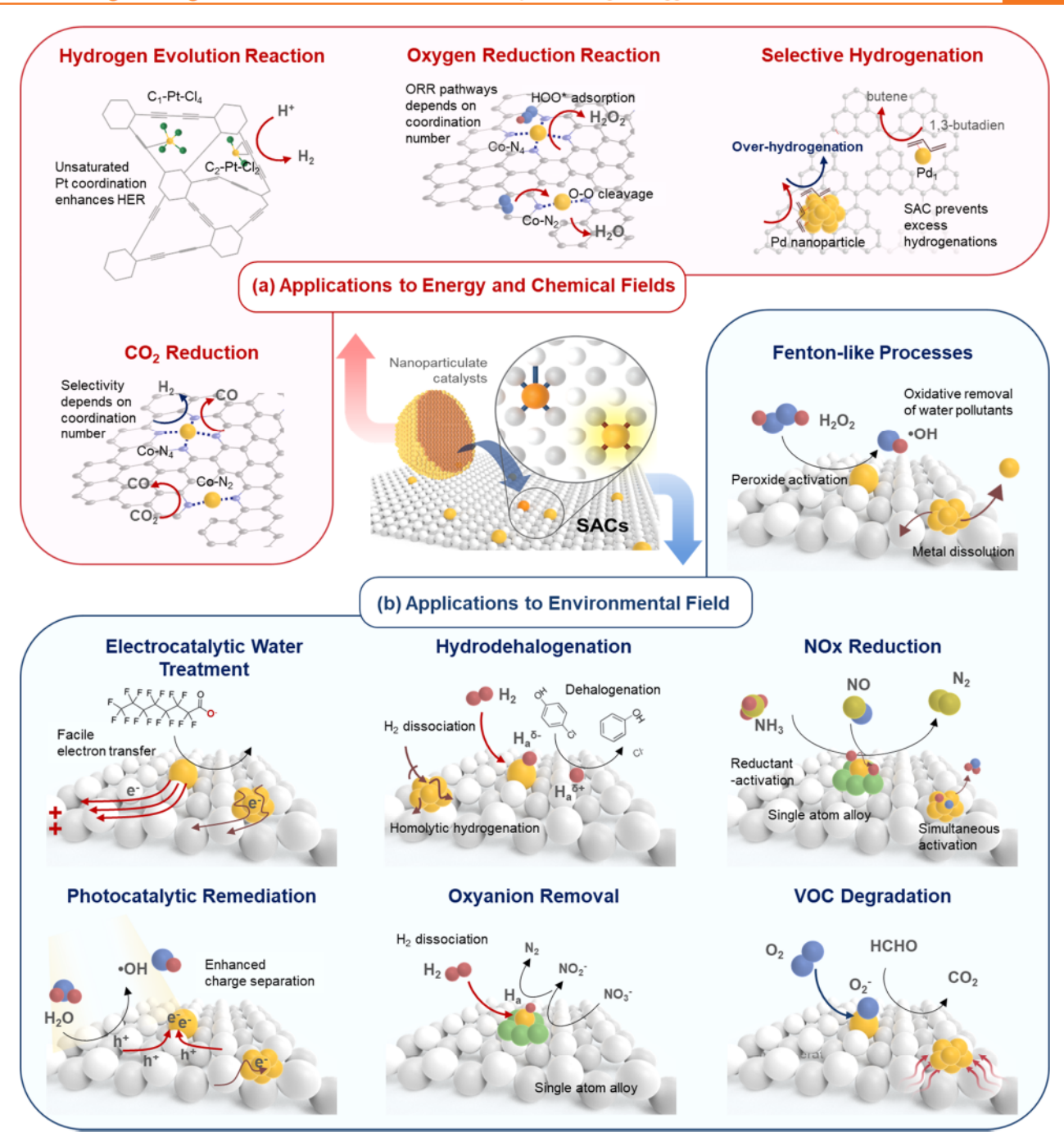


Figure 4. Emerging applications of SACs to (a) energy production and chemical synthesis, such as the hydrogen evolution reaction,  $CO_2$  reduction, oxygen reduction reaction, and selective hydrogenation, and (b) environmental fields such as Fenton-like processes, electrocatalytic water treatment, photocatalytic remediation, hydrodehalogenation, oxyanion removal,  $NO_X$  reduction, and VOC degradation.

discerns the oxidation state, local structure, and coordination environment of the metal atoms. 68,89 For certain metals, CO is not an optimal probe molecule due to its weak adsorption capability and an alternative probe compound should be used. As CO interacts differently with these various metal sites, the energy of its vibrational frequency yields a unique signature that enables the identification of the type of metal sites present in the material. The CO adsorption peak for single-atom catalysts, wherein the metal atoms should only exist in one state, should have a narrow, sharp peak, and the peak for metal clusters or nanoparticles should be broader due to the metal existing in a variety of states (e.g., corners, defects,

or extended surfaces) (Figure 3d). The full width at half-maximum (fwhm) value distinguishes the extent of peak sharpness or broadness, with fwhm values around 5 cm<sup>-1</sup> indicating that the peak is narrow and that the metal species are uniform and exist in the same state.<sup>91</sup>

Once single-atom formation is verified, elemental analysis, such as inductively coupled plasma mass spectrometry (ICP-MS), can be performed to quantify the loading of SACs on support materials. This information is critical to quantitatively compare the atomic efficiency and turnover frequency (TOF; moles of product formed per active metal atom per unit time) of SACs to that of their nanoparticle counterparts. Collectively,

the above analyses provide a comprehensive understanding of the physical dispersion and heterogeneity, chemical structure, coordination environment, and loading amounts of SACs. These characteristics can be correlated to the results of catalytic activity tests to gain insight into the role of SAC material properties in various applications.

# SAC APPLICATIONS TO ENERGY AND CHEMICAL FIELDS

While Pt-based nanomaterials have long been considered the premier catalysts in the electrochemical hydrogen evolution reaction (HER), <sup>92</sup> recent studies suggest that single-atom Pt catalysts can exceed their performance. It has been reported that atomically dispersed Pt catalysts exhibited at least 10 times higher performance for HER than commercial Pt/C catalysts on a Pt mass basis. <sup>44,51,93–95</sup> In addition to HER, SACs have been actively explored for the catalysis of several green chemistry reactions, including the oxygen reduction reaction (ORR), <sup>96–98</sup> CO<sub>2</sub> reduction, <sup>99,100</sup> and the water–gas shift reaction. <sup>58,101</sup> Their improved catalytic activity is often quantitatively evaluated in terms of enhanced TOF. <sup>102,103</sup> Recently, the superior performance and reaction selectivity of SACs for various energy applications have been interpreted in relation to their properties beyond a fundamental understanding of maximized atomic utilization. <sup>104,105</sup>

The unique properties of SACs play a crucial role in increasing target reaction selectivity for sustainable energy applications (Figure 4a). Therefore, SACs must be carefully characterized beyond a simple confirmation of single-atom dispersion. For example, depending on the synthetic scheme, four-coordinated single-atom Pt could be produced on graphdiyne (Pt<sub>1</sub>/GDY2), which demonstrated a much improved HER performance compared to five-coordinated single-atom Pt on graphdiyne (Pt<sub>1</sub>/GDY1) and the commercial Pt/C catalyst. 106 The change of coordination environment led to a greater unoccupied density of 5d orbital of Pt, reducing the Gibbs free energy to near zero to facilitate the adsorption of hydrogen atoms onto Pt SACs. Additionally, compared to Pt nanoparticles, Pt SACs loaded onto WO3-x exhibited an enhanced hydrogen spillover effect due to the strong metalsupport interaction between Pt and WO3-X. Consequently, Pt SACs showed a significantly improved HER performance compared to Pt nanoparticles on  $\hat{WO}_{3-X}$ .

The effects of tunable SAC properties on reaction selectivity are highlighted in ORR performance to yield different final products. The ORR consists of multiple reaction pathways and proceeds either by a four-electron transfer to reduce O2 directly to  $H_2O$   $(O_2 + 4H^+ + 4e^- \rightarrow 2H_2O)$ , a reaction used in fuel cell applications, or by a two-electron transfer to produce  $H_2O_2$   $(O_2 + * + H^+ + e^- \rightarrow HOO^*$  followed by  $HOO^* + (H^+) + e^- \rightarrow H_2O_2 + *$ , where \* denotes unoccupied active catalytic sites), 108 a reaction critical for alternative fuel synthesis. The selectivity is primarily determined by the catalyst's propensity to break the O-O bond of molecular oxygen. 109 The greater capability of catalysts to break O-O bonds enhances the production of the intermediates for fourelectron ORR, i.e., O\* and HO\*. Since HOO\* is the sole intermediate for two-electron ORR, the adsorption energy of HOO\* is the key selectivity indicator for H<sub>2</sub>O<sub>2</sub> production. In particular, it has been reported that controlling the coordination number of SACs with neighboring nitrogen atoms in M-N-C catalysts can selectively tune the pathway of ORR.46 For example, single-atom-loaded Co-N-C catalysts

with a Co– $\rm N_2$  structure promoted the cleavage of O–O bonds and enhanced ORR activity for the four-electron transfer. <sup>96</sup> On the other hand, single-atom Co–N–C catalysts with a Co– $\rm N_4$  structure <sup>110</sup> exhibited superior two-electron selectivity, with over 82% to  $\rm H_2O_2$  production, since electron-deficient cobalt SACs coordinated with four nitrogen atoms act as an active center for adsorbing HOO\*.

In the same way, the properties of SACs greatly influence the selectivity of chemical transformations by tuning reaction pathways. In the selective hydrogenation of acetylene to ethylene (C2H4), the improved performance of single-atom Pd embedded in a Cu ensemble was attributed to the weaker adsorption of C2H4 to the single atom compared to its Pd nanoparticle counterpart, which prevented overhydrogenation to the undesirable ethane product. 111 In the selective hydrogenation of 1,3-butadiene to butene, single-atom Pd loaded on graphene showed complete transformation selectivity, while Pd nanoparticles inevitably exhibited overhydrogenation reactions. 50 It is also important to note that the coordination number of SACs can also determine the selectivity of the chemical transformations. For example, among atomically dispersed Fe-N-C catalysts with different  $FeN_X$  (X = 4-6) structures, 43 the  $FeN_S$  structure exhibited a remarkably selective oxidation efficiency of C-H bonds, a key reaction in the fine chemical industry, over 3 and 10 times higher than that of FeN<sub>6</sub> and FeN<sub>4</sub> coordination, respectively. In addition, the coordination number of SACs was found to affect the electrochemical CO<sub>2</sub> reduction pathway, as shown by atomically dispersed Co-N-C catalysts exhibiting enhanced activity and selectivity toward CO production from CO2 as the Co-N coordination number decreases from 4 to 2. 112 For Co-N<sub>4</sub>, H<sub>2</sub> formation and CO<sub>2</sub> reduction compete with each other due to high  $CO_2^{\bullet-}$  and H adsorption energies. Decreased coordination to N, however, results in more unoccupied 3d orbitals of Co atoms, which is favorable for  $CO_2^{\bullet-}$  adsorption.

In many SAC studies, theoretical analyses by density functional theory (DFT) are performed to calculate the feasibility of target chemical reactions and to deepen the understanding of the role of SACs and their supports, as well as their interaction with reactants and products. Identifying the minimum energy pathway for the reaction and evaluating charge transfer mechanisms are common examples. The predictive and analytical abilities of DFT soundly align with SACs, which have well-defined structures, limited number of active sites, and restricted numbers of possible reaction pathway branches. This is critical because of the high computational cost of DFT which scales, at best, with the number of electrons cubed and a large pre-exponential factor. For example, the restriction of SAC configurations makes calculating all the possible pathways computationally manageable, while minimizing the possibility of overlooking reaction pathways at obscure sites. This is in contrast to metallic nanoparticles where the large size of the particles forces theorists to limit the studies to well-defined surfaces, usually low Miller index planes or simple edges between the metal and support. Therefore, chemical depth can often be overlooked in the interest of computational tractability, which can lead to systematic errors. 113

DFT simulations can also produce quantitative structural information on coordination numbers, bond lengths, bond angles, bonding energies, and the charge density distributions of SACs in order to guide SAC development. For example, on

the basis of the computational hydrogen evolution model, the free energy for hydrogen adsorption ( $\Delta G_{H*}$ ) is widely accepted as a descriptor of the HER process. The calculated  $\Delta G_{H*}$  of an ideal HER catalyst is known to be zero. 114 Referring to the previous example of Pt SACs for HER, the  $\Delta G_{H*}$  of Pt<sub>1</sub>/GDY2 is 0.092 eV, which is extremely close to zero compared to that of Pt<sub>1</sub>/GDY1 ( $\Delta G_{H^*} = -0.653$  eV) and consistent with experimental data showing enhanced HER of Pt<sub>1</sub>/GDY2. In the same way, computationally estimated free energy of OOH adsorption ( $\Delta G_{OOH*}$ ) has been employed to determine the selectivity of ORR for H2O2 production by SACs. The O-O bond length of adsorbed oxygen on each SAC can be another indicator to predict the selective pathway of ORR. SACs with higher O2 binding energy, for example, are more suitable for the selective production of  $H_2O_2$  by elongating O-O bonding and promoting dissociation. The applications of SACs to chemical transformations have been extensively investigated to date, and their prospects continue to be promising for sustainable fuel production, green chemistry (e.g., CO2 reduction), and various reactions that are relevant to environmental applications (such as hydrogenation discussed further below). SACs have changed the perceptions of the functions and challenges of metal-based catalysts and offer opportunities for the selective production of value-added chemicals and more efficient energy production. The development of a deep-learning algorithm is expected to further drive DFT analyses to predict SAC-mediated complex reactions. 116 In addition to the applications mentioned in this review, SACs can be applied beyond such boundaries to catalytic reactions involving complex chemical media.

# SAC APPLICATIONS TO ENVIRONMENTAL FIELDS

Studies on SACs tailored for environmental remediation are in their early stages, with both significant opportunities and challenges lying ahead. Translating the success of SACs in other fields discussed above to environmental applications, such as polluted air and water treatment, is largely uncharted territory despite some similarities in underlying catalytic mechanisms. Current literature clearly suggests that the opportunities for enhanced catalytic activity and selectivity are highly dependent on the types of target reactions and their mechanisms. SAC properties (e.g., the coordination environment of the metal atom, adsorptive interaction with reactants and intermediates, and charge interaction between the metal and support) have complex effects on SAC performance in environmental applications. Here, by matching the practical needs of environmental remediations and the advantageous properties of SACs based on their fundamental catalytic mechanisms discussed above, we identify seven potential environmental applications where SACs may outperform existing catalysts (Figure 4b).

Fenton-like Processes. The redox cycling of transition metals, such as a dissolved Fe<sup>2+</sup>/Fe<sup>3+</sup> pair in a traditional Fenton reaction and various transition metal oxide nanoparticles in heterogeneous Fenton-like reactions, is one of the key mechanisms for the activation of peroxide-containing precursor oxidants such as H<sub>2</sub>O<sub>2</sub> and persulfate (e.g., peroxymonosulfate (PMS) and peroxydisulfate (PDS)). This peroxide activation results in on-site generation of highly reactive, and hence short-lived, radicals such as \*OH and SO<sub>4</sub>\*- that efficiently degrade a wide range of pollutants in advanced oxidation processes (AOPs). The redox reactions involved in the peroxide activation can be accomplished using

SACs that function like dissolved metals while bound to the surface. For example, single-atom-Fe-loaded mesoporous silica with a Fe-O<sub>4</sub> structure was found to exhibit superior catalytic activity compared to Fe nanoparticles for H<sub>2</sub>O<sub>2</sub> activation and subsequent phenol degradation. Reduced adsorption energy and facilitated electron transfer to PMS induced by properties of SACs enhanced sulfate radical production and pollutant degradation. Considering the extensive literature on Fenton-like processes involving both homogeneous and heterogeneous catalysts as well as various precursors, SAC research has tremendous potential in this subject.

Electrocatalytic Water Treatment. Electrocatalytic processes involving radical generation and direct electrode reactions (e.g., anodic oxidation of pollutants) are not yet widely employed for water treatment. A need for developing electrode materials and architecture with improved performance and stability as well as reduced cost has been identified as one of the major challenges for these applications, but only a few studies have attempted to use SACs in place of benchmark nanocatalysts. 119,120 An N-doped graphene conductive membrane loaded with single-atom cobalt 121 and a Ti<sub>4</sub>O<sub>7</sub> electrode loaded with Pd single atoms 122 are early examples of SACs showing enhanced and selective anodic oxidation of organic pollutants. It should be noted that SACs have been extensively employed to improve the kinetics and selectivity of electrode materials in various other electrochemical processes, including ORR, <sup>123–125</sup> OER, <sup>126</sup> HER, <sup>127,128</sup> and hydrocarbon conversion reactions. 102 Strong catalyst binding with the support, enhanced charge transfer, and tailoring of reaction mechanisms through the concerted contribution of support materials may explain SAC's ability to outperform nanoparticle counterparts. Ample research opportunities exist to translate these findings to electrochemical water treatment.

Photocatalytic Remediation. SACs have likewise been emerging as a viable strategy to enhance the performance of semiconductor photocatalysts by modifying their light absorption and charge separation properties. 129 For example, incorporating single atoms Pt, Pd, Au, and Cu into C<sub>3</sub>N<sub>4</sub> was found to lower the bandgap energy of C<sub>3</sub>N<sub>4</sub> and therefore enhance the absorption of lower energy photons such as visible light. 130,131 Similar to conductive nanoparticles that are often loaded onto semiconductors, several recent studies also indicated improved charge separation by metal single atoms, which was attributed to their more efficient loading due to strong metal-ligand interactions and shortened charge transfer distances (i.e., from a light harvesting unit to a catalytic site). These strategies have been extrapolated to photocatalysts used for water treatment; for example, loading Fe and Ag single atoms onto semiconductors such as C<sub>3</sub>N<sub>4</sub> and  ${
m TiO_2}$  enhanced light absorption, radical generation, and subsequent pollutant degradation. Considering the vast options available for semiconductor materials and SAC configurations, the opportunity to explore SACs for photocatalytic water and air treatment and to advance fundamental knowledge appears great. Future research, however, requires a careful scrutiny of its true potential for real world applications, since incremental improvements in material properties are unlikely to significantly advance photocatalysis practice in water treatment. 140

Hydrodehalogenation. Organohalogens remain as one group of the most persistent and widespread water contaminants due to the strength of their carbon-halogen bonds. Halogenated organics occur widely as agrochemicals,

I

pharmaceuticals, solvents, surfactants, and byproducts in hydraulic fracturing wastewater and chlorine-disinfected water. The adverse effects of many halogenated organics on human health and the ecosystem have been well-documented, and several of these organics are currently regulated. <sup>141</sup> Due to the difficulty of destroying these persistent pollutants by chemical and biological processes commonly employed in water treatment, <sup>142,143</sup> a reductive dehalogenation scheme, i.e., cleaving the C–X (where X is F, Cl, Br, or I) bonds by H atoms, has been pursued as a viable alternative.

In typical hydrogeneration processes, hydrogen atoms are produced by the dissociation of H2 on the surface of noble metal nanoparticles. However, this homolytic process generates hydrogen atoms that are not selective for C-X bond hydrogenation and are also likely to partake in the reduction of other electron-rich functionalities, such as C=C bonds in target molecules and interfering species like natural organic matter. Tailoring the architecture of SACs is expected to play a crucial role in achieving higher catalytic selectivity by promoting an alternative heterolytic pathway, forming two distinct partially charged  $H^{\delta-}$  and  $H^{\delta+}$  atoms through H atom spillover immediately after H<sub>2</sub> dissociation. 70,145 The H<sup>δ-</sup> and  $H^{\delta+}$  pair can preferentially align with the polar carbon—halogen bond, instead of the nonpolar C=C bond, to achieve higher rates of the selective hydrogenation of C-X bonds. Alternatively, H atoms can be photocatalytically generated from proton reduction on SACs, for example, on single-atom-Pt-loaded SiC, as demonstrated by its successful hydrodefluorination of perfluorooctanoic acid (PFOA),71 one of the poly- and perfluoroalkyl substances (PFAS) of emerging concern. The superior performance and tunable selectivity of SACs, which has been shown in the hydrogenation of alkynes, 146,147 diene, 50 styrene, 148 and benzaldehyde, 70 can be useful for the selective removal of organohalogens in aquatic

Oxyanion Removal. Oxyanions (NO<sub>3</sub><sup>-</sup>, NO<sub>2</sub><sup>-</sup>, BrO<sub>3</sub><sup>-</sup>, CrO<sub>4</sub><sup>2-</sup>, ClO<sub>4</sub><sup>-</sup>, etc.) are widespread drinking water contaminants that are highly soluble, mobile in water, and challenging to remove. Reducing oxyanions with bimetallic Pd-based catalysts has garnered significant attention due to their high activity, stability, and selectivity for the desired end product. 19,149 The key reaction step for the catalytic reduction of oxyanions using metal nanoparticles is the dissociation of adsorbed H<sub>2</sub> into H atoms, similar to hydrodehalogenation. Past studies suggest that the efficiency of oxyanion reduction using Pd strongly depends on the type of oxyanion, generally following the order  $CrO_4^{2-} > NO_2^{-} > BrO_3^{-} \gg ClO_4^{-} > NO_3^{-}$ , in terms of the ease of reduction. In addition to the difficulty of reduction, nitrate poses serious human health threats, such as an increased risk of cancer and birth defects. 151 Among the various catalytic materials proposed, bimetallic Pd catalysts alloyed with Cu, which can act as a promoter metal to transform nitrate to nitrite, is widely accepted as one of the most active and selective catalysts for nitrate reduction. 152 Similarly, SAAs may have the potential to replace the role of bimetallic catalysts by maximizing the atomic efficiency of both

 $NO_X$  Reduction. The selective catalytic reduction (SCR) of  $NO_X$  (DeNO<sub>X</sub>) is a key process in the purification of automotive, industrial, and boiler gas exhausts. Conventional DeNO<sub>X</sub> processes, which involve reactions with reductants such as  $H_2$  and  $NH_3$  over noble metal catalysts, typically have a relatively high-energy barrier and therefore proceed efficiently

only at high temperatures. Recent computational studies point toward the possibility of bimetallic catalysts in SAA architectures, for example, single-atom-Ir-doped Ni to achieve high-efficiency, low-temperature SCR. <sup>154</sup> In SAAs, the substantially lowered energy barrier for H<sub>2</sub> dissociation at the noble metal site and subsequent desorption from the host metal surface can lower the reaction temperature. <sup>148</sup> In addition, the cleavage of N–O bonds in adsorbed (NO)<sub>2</sub> dimers, which is a rate-determining step for NO reduction, can be accelerated by single Pd on a Cu alloy, yielding superior N<sub>2</sub> selectivity, even in mixed exhaust gases. <sup>155</sup> DeNO<sub>x</sub> presents a significant opportunity for SACs as exemplified by recent advances, such as single Rh on Al<sub>2</sub>O<sub>3</sub> and CeO<sub>2</sub> <sup>156</sup> and single Pd on CeO<sub>2</sub>. <sup>157</sup> Additionally, other gas phase catalytic reactions, such as CO oxidation, have already seen significant progress with SACs. <sup>158</sup>

VOC Degradation. Catalytic decomposition is a promising approach to alleviate indoor air pollution by volatile organic compounds (VOCs), such as formaldehyde and toluene, which cannot be removed by common air filters. Significant progress has been achieved in catalytically decomposing, for example, formaldehyde to carbon dioxide, at room temperature by noble metal catalysts. 159,160 However, effective decomposition of aromatic VOCs, such as toluene and benzene, still requires high temperatures or external energy, presenting great challenges for practical indoor air purification. 161 Since the formation of ROS on the catalyst surface by O2 activation is often the rate-limiting step of catalytic VOC degradation, catalysts that reduce the activation energy of molecular oxygen should be designed. 162 It was recently reported that singleatom Pt deposited on MnO2 can degrade toluene at room temperature by efficiently producing surface lattice oxygen and OH radicals. 163 Unlike in aqueous reactions, the catalyst surface is gradually covered by recalcitrant organic intermediates, so further investigation should be undertaken to study the SAC environment, which is resistant to catalyst deactivation. 164

# ■ PROSPECT AND CHALLENGES

SACs have several features that are particularly appealing to environmental remediation applications. The high costs of nanomaterials, either due to the high cost of raw materials (e.g., noble metals) or high cost of synthesis (e.g., thermal processes), have been significantly limiting to their adoption to real world practice, despite over two decades of research in adopting nanotechnology for environmental catalysis.<sup>20</sup> On the contrary, extremely low consumption of raw materials and lowcost synthesis procedures can significantly relieve the economic burden, potentially initiating a new era of environmental catalysis in which the cost of noble metals is no longer an issue. It is time to reexamine and reevaluate various environmental materials that have been limited due to the cost of noble metals. Another significant challenge of employing nanomaterials in environmental applications is their potential release and impact on the environment and human health, even when nanomaterials are immobilized onto larger substrates, due to the concern of leaching. In contrast, it is expected that SACs are much more stable and less prone to leach because each catalytic center is covalently bound to the substrate, though future research is required to verify this hypothesis. Even if they are released from the surface, it is likely be in an ionic state rather than as particles. The absolute amount of metal used is also much less than in nanomaterials for a system with

the same target efficiency and capacity. Finally, SACs can drive some reactions that cannot be achieved by nanoparticles, as discussed above (e.g., hydrogenation reactions) due to the differences in size of their catalytic centers as well as the differential contribution of their surrounding environments.

However, SACs are not immune to some challenges that nanomaterials have been facing in environmental applications. Most notably, complex media in the environment contain constituents that are likely to interfere with catalysis via catalyst surface fouling and deactivation. Diminished performance in complex media compared to the simple media typically used in laboratory research imposes high demands on the selectivity of SACs toward pollutant removal reactions. Another challenge is related to how SAC materials can be integrated into reactors and systems that are used in water and air purification. Similar questions have been continuously raised for the use of nanomaterials with few engineering solutions proven successful in industrial practices. In addition, one challenge that is unique to SACs is their potential agglomeration into clusters and the loss of single-atom characteristics over long-term use due to high surface energy. It is possible that this SAC deterioration may also be affected by the surrounding media and specific reactions determined by the redox environment.

Many new developments in science conjure inflated expectations, exemplified by the case of semiconductor photocatalysts in water treatment research, which has been criticized for its sluggish technology translation and commercialization despite extensive investment. 140 It is therefore important to fully appreciate SAC's shortcomings from the beginning of its development, by taking advantage of experience gained through environmental nanotechnology research. In order for SACs to become effective at addressing various aspects of environmental pollution and potentially revolutionize environmental remediation technology, future research should be designed with (i) a clear environmental remediation focus based on needs; (ii) consideration of complex environmental media, especially when adopting recent advances in chemical synthesis and energy production that deal with less complex media; (iii) a careful evaluation of their longterm stability, potentially using in operando characterization techniques<sup>165</sup> and tracking performance over long-term experiments; and (iv) a balanced effort between a deeper understanding of SAC fundamentals and system-level engineering.

# AUTHOR INFORMATION

## Corresponding Author

Jae-Hong Kim — Department of Chemical and Environmental Engineering, Yale University, New Haven, Connecticut 06511, United States; ⊙ orcid.org/0000-0003-2224-3516; Phone: +1-203-432-4386; Email: jaehong.kim@yale.edu; Fax: +1-203-432-4387

#### Authors

Seunghyun Weon — Department of Chemical and Environmental Engineering, Yale University, New Haven, Connecticut 06511, United States; School of Health and Environmental Science, Korea University, Seoul 02841, Korea; orcid.org/0000-0003-4529-8069

Dahong Huang – Department of Chemical and Environmental Engineering, Yale University, New Haven, Connecticut 06S11, United States; oorcid.org/0000-0003-4544-6113

Kali Rigby – Department of Chemical and Environmental Engineering, Yale University, New Haven, Connecticut 06511, United States

Chiheng Chu — Department of Chemical and Environmental Engineering, Yale University, New Haven, Connecticut 06511, United States; Department of Environmental Science, Zhejiang University, Hangzhou 310058, China; orcid.org/0000-0001-9493-9120

Xuanhao Wu — Department of Chemical and Environmental Engineering, Yale University, New Haven, Connecticut 06511, United States; oocid.org/0000-0001-6177-6089

Complete contact information is available at: https://pubs.acs.org/10.1021/acsestengg.0c00136

#### Notes

The authors declare no competing financial interest.

# ACKNOWLEDGMENTS

This study was partly supported the National Science Foundation (NSF) Nanosystems Engineering Research Center for Nanotechnology-Enabled Water Treatment (EEC-1449500) and NSF Division of Chemical, Bioengineering, Environmental, and Transport Systems (CBET) Grant #1955793. D. Huang was funded by the National Science Fund for Distinguished Young Scholars (No. 51625801). The authors also thank Gary Haller and Judy Cha at Yale University and Christopher Muhich at Arizona State University for fruitful discussions.

# REFERENCES

- (1) Haruta, M.; Kobayashi, T.; Sano, H.; Yamada, N. Novel gold catalysts for the oxidation of carbon monoxide at a temperature far below 0 °C. Chem. Lett. 1987, 16 (2), 405–408.
- (2) Turner, M.; Golovko, V. B.; Vaughan, O. P. H.; Abdulkin, P.; Berenguer-Murcia, A.; Tikhov, M. S.; Johnson, B. F. G.; Lambert, R. M. Selective oxidation with dioxygen by gold nanoparticle catalysts derived from 55-atom clusters. *Nature* **2008**, *454*, 981–983.
- (3) Loeb, S.; Li, C. H.; Kim, J. H. Solar photothermal disinfection using broadband-light absorbing gold nanoparticles and carbon black. *Environ. Sci. Technol.* **2018**, *52* (1), 205–213.
- (4) Wei, H.; Loeb, S. K.; Halas, N. J.; Kim, J.-H. Plasmon-enabled degradation of organic micropollutants in water by visible-light illumination of Janus gold nanorods. *Proc. Natl. Acad. Sci. U. S. A.* **2020**, *117* (27), 15473–15481.
- (5) Qiao, B.; Wang, A.; Yang, X.; Allard, L. F.; Jiang, Z.; Cui, Y.; Liu, J.; Li, J.; Zhang, T. Single-atom catalysis of CO oxidation using Pt<sub>1</sub>/FeOx. *Nat. Chem.* **2011**, *3* (8), 634–641.
- (6) Lee, B.-H.; Park, S.; Kim, M.; Sinha, A. K.; Lee, S. C.; Jung, E.; Chang, W. J.; Lee, K.-S.; Kim, J. H.; Cho, S.-P. Reversible and cooperative photoactivation of single-atom Cu/TiO<sub>2</sub> photocatalysts. *Nat. Mater.* **2019**, *18*, 620–626.
- (7) Zhu, C.; Shi, Q.; Feng, S.; Du, D.; Lin, Y. Single-atom catalysts for electrochemical water splitting. *ACS Energy Letters* **2018**, 3 (7), 1713–1721.
- (8) Mitchell, S.; Vorobyeva, E.; Pérez-Ramírez, J. The multifaceted reactivity of single-atom heterogeneous catalysts. *Angew. Chem., Int. Ed.* **2018**, *57* (47), 15316–15329.
- (9) Hu, P.; Huang, Z.; Amghouz, Z.; Makkee, M.; Xu, F.; Kapteijn, F.; Dikhtiarenko, A.; Chen, Y.; Gu, X.; Tang, X. Electronic metal—support interactions in single-atom catalysts. *Angew. Chem., Int. Ed.* **2014**, 53 (13), 3418–3421.
- (10) Daelman, N.; Capdevila-Cortada, M.; López, N. Dynamic charge and oxidation state of Pt/CeO<sub>2</sub> single-atom catalysts. *Nat. Mater.* **2019**, *18* (11), 1215–1221.

- (11) Li, Z.; Ji, S.; Liu, Y.; Cao, X.; Tian, S.; Chen, Y.; Niu, Z.; Li, Y. Well-defined materials for heterogeneous catalysis: from nanoparticles to isolated single-atom sites. *Chem. Rev.* **2020**, *120* (2), 623–682.
- (12) Hannagan, R. T.; Giannakakis, G.; Flytzani-Stephanopoulos, M.; Sykes, E. C. H. Single-atom alloy catalysis. *Chem. Rev.* **2020**, DOI: 10.1021/acs.chemrev.0c00078.
- (13) Shan, J.; Li, M.; Allard, L. F.; Lee, S.; Flytzani-Stephanopoulos, M. Mild oxidation of methane to methanol or acetic acid on supported isolated rhodium catalysts. *Nature* **2017**, *551*, 605–608.
- (14) Wei, H.; Liu, X.; Wang, A.; Zhang, L.; Qiao, B.; Yang, X.; Huang, Y.; Miao, S.; Liu, J.; Zhang, T. FeOx-supported platinum single-atom and pseudo-single-atom catalysts for chemoselective hydrogenation of functionalized nitroarenes. *Nat. Commun.* 2014, 5, 5634.
- (15) Yang, H. B.; Hung, S.-F.; Liu, S.; Yuan, K.; Miao, S.; Zhang, L.; Huang, X.; Wang, H.-Y.; Cai, W.; Chen, R. Atomically dispersed Ni(I) as the active site for electrochemical CO<sub>2</sub> reduction. *Nature Energy* **2018**, 3 (2), 140.
- (16) Cao, L.; Luo, Q.; Liu, W.; Lin, Y.; Liu, X.; Cao, Y.; Zhang, W.; Wu, Y.; Yang, J.; Yao, T. Identification of single-atom active sites in carbon-based cobalt catalysts during electrocatalytic hydrogen evolution. *Nature Catalysis* **2019**, 2 (2), 134.
- (17) Li, Y.; Somorjai, G. A. Nanoscale advances in catalysis and energy applications. *Nano Lett.* **2010**, *10* (7), 2289–2295.
- (18) Liu, Y.; Zhou, G.; Liu, K.; Cui, Y. Design of complex nanomaterials for energy storage: past success and future opportunity. *Acc. Chem. Res.* **2017**, *50* (12), 2895–2905.
- (19) Chaplin, B. P.; Reinhard, M.; Schneider, W. F.; Schüth, C.; Shapley, J. R.; Strathmann, T. J.; Werth, C. J. Critical review of Pd-based catalytic treatment of priority contaminants in water. *Environ. Sci. Technol.* **2012**, *46* (7), 3655–3670.
- (20) Mauter, M. S.; Zucker, I.; Perreault, F.; Werber, J. R.; Kim, J.-H.; Elimelech, M. The role of nanotechnology in tackling global water challenges. *Nature Sustainability* **2018**, *1* (4), 166–175.
- (21) Guo, S.; Heck, K.; Kasiraju, S.; Qian, H.; Zhao, Z.; Grabow, L. C.; Miller, J. T.; Wong, M. S. Insights into nitrate reduction over indium-decorated palladium nanoparticle catalysts. *ACS Catal.* **2018**, 8 (1), 503–515.
- (22) Li, H.; Guo, S.; Shin, K.; Wong, M. S.; Henkelman, G. Design of a Pd-Au nitrite reduction catalyst by identifying and optimizing active ensembles. *ACS Catal.* **2019**, *9* (9), 7957–7966.
- (23) Wang, Y.; Liu, J.; Wang, P.; Werth, C. J.; Strathmann, T. J. Palladium nanoparticles encapsulated in core—shell silica: a structured hydrogenation catalyst with enhanced activity for reduction of oxyanion water pollutants. ACS Catal. 2014, 4 (10), 3551–3559.
- (24) Fei, H.; Dong, J.; Chen, D.; Hu, T.; Duan, X.; Shakir, I.; Huang, Y.; Duan, X. Single atom electrocatalysts supported on graphene or graphene-like carbons. *Chem. Soc. Rev.* **2019**, *48* (20), 5207–5241.
- (25) Ding, S.; Hülsey, M. J.; Pérez-Ramírez, J.; Yan, N. Transforming energy with single-atom catalysts. *Joule* **2019**, 3 (12), 2897–2929.
- (26) Zhang, L.; Doyle-Davis, K.; Sun, X. Pt-Based electrocatalysts with high atom utilization efficiency: from nanostructures to single atoms. *Energy Environ. Sci.* **2019**, 12 (2), 492–517.
- (27) Zhang, L.; Zhou, M.; Wang, A.; Zhang, T. Selective hydrogenation over supported metal catalysts: from nanoparticles to single atoms. *Chem. Rev.* **2020**, *120* (2), *683*–733.
- (28) Ji, S.; Chen, Y.; Wang, X.; Zhang, Z.; Wang, D.; Li, Y. Chemical synthesis of single atomic site catalysts. *Chem. Rev.* **2020**, DOI: 10.1021/acs.chemrev.9b00818.
- (29) Zhang, L.; Ren, Y.; Liu, W.; Wang, A.; Zhang, T. Single-atom catalyst: a rising star for green synthesis of fine chemicals. *National Science Review* **2018**, *5* (5), 653–672.
- (30) Wang, A.; Li, J.; Zhang, T. Heterogeneous single-atom catalysis. *Nature Reviews Chemistry* **2018**, 2 (6), 65–81.
- (31) Yang, X.-F.; Wang, A.; Qiao, B.; Li, J.; Liu, J.; Zhang, T. Singleatom catalysts: a new frontier in heterogeneous catalysis. *Acc. Chem. Res.* 2013, 46 (8), 1740–1748.

- (32) Liu, L.; Corma, A. Metal catalysts for heterogeneous catalysis: from single atoms to nanoclusters and nanoparticles. *Chem. Rev.* **2018**, *118* (10), 4981–5079.
- (33) Campbell, C. T. Catalyst-support interactions: electronic perturbations. *Nat. Chem.* **2012**, *4* (8), 597–598.
- (34) Li, X.; Huang, X.; Xi, S.; Miao, S.; Ding, J.; Cai, W.; Liu, S.; Yang, X.; Yang, H.; Gao, J.; Wang, J.; Huang, Y.; Zhang, T.; Liu, B. Single cobalt atoms anchored on porous N-doped graphene with dual reaction sites for efficient Fenton-like catalysis. *J. Am. Chem. Soc.* 2018, 140 (39), 12469–12475.
- (35) Jirkovský, J. S.; Panas, I.; Ahlberg, E.; Halasa, M.; Romani, S.; Schiffrin, D. J. Single atom hot-spots at Au–Pd nanoalloys for electrocatalytic H<sub>2</sub>O<sub>2</sub> Production. J. Am. Chem. Soc. **2011**, 133 (48), 19432–19441.
- (36) Yang, S.; Tak, Y. J.; Kim, J.; Soon, A.; Lee, H. Support effects in single-atom platinum catalysts for electrochemical oxygen reduction. *ACS Catal.* **2017**, *7* (2), 1301–1307.
- (37) Qin, R.; Liu, K.; Wu, Q.; Zheng, N. Surface coordination chemistry of atomically dispersed metal catalysts. *Chem. Rev.* **2020**, DOI: 10.1021/acs.chemrev.0c00094.
- (38) Nie, L.; Mei, D.; Xiong, H.; Peng, B.; Ren, Z.; Hernandez, X. I. P.; DeLaRiva, A.; Wang, M.; Engelhard, M. H.; Kovarik, L.; Datye, A. K.; Wang, Y. Activation of surface lattice oxygen in single-atom Pt/CeO<sub>2</sub> for low-temperature CO oxidation. *Science* **2017**, 358 (6369), 1419–1423.
- (39) Ding, K.; Gulec, A.; Johnson, A. M.; Schweitzer, N. M.; Stucky, G. D.; Marks, L. D.; Stair, P. C. Identification of active sites in CO oxidation and water-gas shift over supported Pt catalysts. *Science* **2015**, 350 (6257), 189–192.
- (40) Kopelent, R.; van Bokhoven, J. A.; Szlachetko, J.; Edebeli, J.; Paun, C.; Nachtegaal, M.; Safonova, O. V. Catalytically active and spectator Ce<sup>3+</sup> in ceria-supported metal catalysts. *Angew. Chem., Int. Ed.* **2015**, *54* (30), 8728–8731.
- (41) Cargnello, M.; Doan-Nguyen, V. V. T.; Gordon, T. R.; Diaz, R. E.; Stach, E. A.; Gorte, R. J.; Fornasiero, P.; Murray, C. B. Control of metal nanocrystal size reveals metal-support interface role for ceria catalysts. *Science* **2013**, *341* (6147), 771–773.
- (42) Allian, A. D.; Takanabe, K.; Fujdala, K. L.; Hao, X.; Truex, T. J.; Cai, J.; Buda, C.; Neurock, M.; Iglesia, E. Chemisorption of CO and mechanism of CO oxidation on supported platinum nanoclusters. *J. Am. Chem. Soc.* **2011**, 133 (12), 4498–4517.
- (43) Liu, W.; Zhang, L.; Liu, X.; Liu, X.; Yang, X.; Miao, S.; Wang, W.; Wang, A.; Zhang, T. Discriminating catalytically active FeNx species of atomically dispersed Fe-N-C catalyst for selective oxidation of the C-H bond. J. Am. Chem. Soc. 2017, 139 (31), 10790-10798.
- (44) Ren, Y.; Tang, Y.; Zhang, L.; Liu, X.; Li, L.; Miao, S.; Sheng Su, D.; Wang, A.; Li, J.; Zhang, T. Unraveling the coordination structure-performance relationship in Pt<sub>1</sub>/Fe<sub>2</sub>O<sub>3</sub> single-atom catalyst. *Nat. Commun.* **2019**, *10* (1), 4500.
- (45) Gong, Y. N.; Jiao, L.; Qian, Y.; Pan, C. Y.; Zheng, L.; Cai, X.; Liu, B.; Yu, S. H.; Jiang, H. L. Regulating the coordination environment of MOF-templated single-atom nickel electrocatalysts for boosting  ${\rm CO_2}$  reduction. *Angew. Chem., Int. Ed.* **2020**, 59 (7), 2705–2709.
- (46) Yin, P.; Yao, T.; Wu, Y.; Zheng, L.; Lin, Y.; Liu, W.; Ju, H.; Zhu, J.; Hong, X.; Deng, Z. Single cobalt atoms with precise N-coordination as superior oxygen reduction reaction catalysts. *Angew. Chem., Int. Ed.* **2016**, *55* (36), 10800–10805.
- (47) Liu, P.; Zheng, N. Coordination chemistry of atomically dispersed catalysts. *National Science Review* **2018**, 5 (5), 636–638.
- (48) Zhang, H.; Li, J.; Xi, S.; Du, Y.; Hai, X.; Wang, J.; Xu, H.; Wu, G.; Zhang, J.; Lu, J.; Wang, J. A graphene-supported single-atom FeN<sub>5</sub> catalytic site for efficient electrochemical CO<sub>2</sub> reduction. *Angew. Chem., Int. Ed.* **2019**, 58 (42), 14871–14876.
- (49) Sun, S.; Zhang, G.; Gauquelin, N.; Chen, N.; Zhou, J.; Yang, S.; Chen, W.; Meng, X.; Geng, D.; Banis, M. N. Single-atom catalysis using Pt/graphene achieved through atomic layer deposition. *Sci. Rep.* 2013, 3, 1775.

- (50) Yan, H.; Cheng, H.; Yi, H.; Lin, Y.; Yao, T.; Wang, C.; Li, J.; Wei, S.; Lu, J. Single-atom Pd<sub>1</sub>/graphene catalyst achieved by atomic layer deposition: remarkable performance in selective hydrogenation of 1, 3-butadiene. *J. Am. Chem. Soc.* **2015**, *137* (33), 10484–10487.
- (51) Cheng, N.; Stambula, S.; Wang, D.; Banis, M. N.; Liu, J.; Riese, A.; Xiao, B.; Li, R.; Sham, T.-K.; Liu, L.-M.; Botton, G. A.; Sun, X. Platinum single-atom and cluster catalysis of the hydrogen evolution reaction. *Nat. Commun.* **2016**, *7* (1), 13638.
- (52) Abbet, S.; Sanchez, A.; Heiz, U.; Schneider, W.-D.; Ferrari, A. M.; Pacchioni, G.; Rösch, N. Acetylene cyclotrimerization on supported size-selected Pd n clusters ( $1 \le n \le 30$ ): one atom is enough! *J. Am. Chem. Soc.* **2000**, *122* (14), 3453–3457.
- (53) Kaden, W. E.; Wu, T.; Kunkel, W. A.; Anderson, S. L. Electronic structure controls reactivity of size-selected Pd clusters adsorbed on TiO<sub>2</sub> surfaces. *Science* **2009**, 326 (5954), 826–829.
- (54) Yoon, B.; Häkkinen, H.; Landman, U.; Wörz, A. S.; Antonietti, J.-M.; Abbet, S.; Judai, K.; Heiz, U. Charging effects on bonding and catalyzed oxidation of CO on Au<sub>8</sub> clusters on MgO. *Science* **2005**, 307 (5708), 403–407.
- (55) Yan, H.; Su, C.; He, J.; Chen, W. Single-atom catalysts and their applications in organic chemistry. *J. Mater. Chem. A* **2018**, 6 (19), 8793–8814.
- (56) Gu, X.-K.; Qiao, B.; Huang, C.-Q.; Ding, W.-C.; Sun, K.; Zhan, E.; Zhang, T.; Liu, J.; Li, W.-X. Supported single Pt<sub>1</sub>/Au<sub>1</sub> atoms for methanol steam reforming. *ACS Catal.* **2014**, *4* (11), 3886–3890.
- (57) Moses-DeBusk, M.; Yoon, M.; Allard, L. F.; Mullins, D. R.; Wu, Z.; Yang, X.; Veith, G.; Stocks, G. M.; Narula, C. K. CO oxidation on supported single Pt atoms: experimental and ab initio density functional studies of CO interaction with Pt atom on  $\theta$ -Al<sub>2</sub>O<sub>3</sub>(010) surface. *J. Am. Chem. Soc.* **2013**, *135* (34), 12634–12645.
- (58) Lin, L.; Zhou, W.; Gao, R.; Yao, S.; Zhang, X.; Xu, W.; Zheng, S.; Jiang, Z.; Yu, Q.; Li, Y.-W. Low-temperature hydrogen production from water and methanol using  $Pt/\alpha$ -MoC catalysts. *Nature* **2017**, 544, 80–83.
- (59) Jiao, L.; Jiang, H.-L. Metal-organic-framework-based singleatom catalysts for energy applications. *Chem.* **2019**, *5* (4), 786–804.
- (60) Zhang, X.; Chen, A.; Zhong, M.; Zhang, Z.; Zhang, X.; Zhou, Z.; Bu, X.-H. Metal-organic frameworks (MOFs) and MOF-derived materials for energy storage and conversion. *Electrochemical Energy Reviews* **2019**, 2 (1), 29–104.
- (61) Abdel-Mageed, A. M.; Rungtaweevoranit, B.; Parlinska-Wojtan, M.; Pei, X.; Yaghi, O. M.; Behm, R. J. Highly active and stable single-atom Cu catalysts supported by a metal—organic framework. *J. Am. Chem. Soc.* **2019**, *141* (13), 5201–5210.
- (62) Zhong, W.; Sa, R.; Li, L.; He, Y.; Li, L.; Bi, J.; Zhuang, Z.; Yu, Y.; Zou, Z. A covalent organic framework bearing single Ni sites as a synergistic photocatalyst for selective photoreduction of CO<sub>2</sub> to CO. *J. Am. Chem. Soc.* **2019**, *141* (18), 7615–7621.
- (63) Yang, M.; Li, S.; Wang, Y.; Herron, J. A.; Xu, Y.; Allard, L. F.; Lee, S.; Huang, J.; Mavrikakis, M.; Flytzani-Stephanopoulos, M. Catalytically active Au-O(OH)x-species stabilized by alkali ions on zeolites and mesoporous oxides. *Science* **2014**, 346 (6216), 1498–1501
- (64) Liu, L.; Díaz, U.; Arenal, R.; Agostini, G.; Concepción, P.; Corma, A. Generation of subnanometric platinum with high stability during transformation of a 2D zeolite into 3D. *Nat. Mater.* **2017**, *16*, 132–138.
- (65) He, T.; Chen, S.; Ni, B.; Gong, Y.; Wu, Z.; Song, L.; Gu, L.; Hu, W.; Wang, X. Zirconium—porphyrin-based metal—organic framework hollow nanotubes for immobilization of noble-metal single atoms. *Angew. Chem., Int. Ed.* **2018**, *57* (13), 3493—3498.
- (66) DeRita, L.; Resasco, J.; Dai, S.; Boubnov, A.; Thang, H. V.; Hoffman, A. S.; Ro, I.; Graham, G. W.; Bare, S. R.; Pacchioni, G.; Pan, X.; Christopher, P. Structural evolution of atomically dispersed Pt catalysts dictates reactivity. *Nat. Mater.* 2019, 18, 746–751.
- (67) Resasco, J.; DeRita, L.; Dai, S.; Chada, J. P.; Xu, M.; Yan, X.; Finzel, J.; Hanukovich, S.; Hoffman, A. S.; Graham, G. W.; Bare, S. R.; Pan, X.; Christopher, P. Uniformity is key in defining structure—

- function relationships for atomically dispersed metal catalysts: the case of Pt/CeO<sub>2</sub>. J. Am. Chem. Soc. 2020, 142 (1), 169–184.
- (68) DeRita, L.; Dai, S.; Lopez-Zepeda, K.; Pham, N.; Graham, G. W.; Pan, X.; Christopher, P. Catalyst architecture for stable single atom dispersion enables site-specific spectroscopic and reactivity measurements of CO adsorbed to Pt atoms, oxidized Pt clusters, and metallic Pt clusters on TiO<sub>2</sub>. J. Am. Chem. Soc. **2017**, 139 (40), 14150–14165.
- (69) Zhao, J.; Chen, Z. Single Mo atom supported on defective boron nitride monolayer as an efficient electrocatalyst for nitrogen fixation: a computational study. *J. Am. Chem. Soc.* **2017**, *139* (36), 12480–12487.
- (70) Liu, P.; Zhao, Y.; Qin, R.; Mo, S.; Chen, G.; Gu, L.; Chevrier, D. M.; Zhang, P.; Guo, Q.; Zang, D. Photochemical route for synthesizing atomically dispersed palladium catalysts. *Science* **2016**, 352 (6287), 797–800.
- (71) Huang, D.; de Vera, G. A.; Chu, C.; Zhu, Q.; Stavitski, E.; Mao, J.; Xin, H.; Spies, J. A.; Schmuttenmaer, C. A.; Niu, J.; Haller, G. L.; Kim, J.-H. Single-atom Pt catalyst for effective C-F bond activation via hydrodefluorination. ACS Catal. 2018, 8 (10), 9353–9358.
- (72) Chu, C. H.; Zhu, Q. H.; Pan, Z. H.; Gupta, S.; Huang, D. H.; Du, Y. H.; Weon, S.; Wu, Y. A.; Muhich, C.; Stavitski, E.; Domen, K.; Kim, J. H. Spatially separating redox centers on 2D carbon nitride with cobalt single atom for photocatalytic H<sub>2</sub>O<sub>2</sub> production. *Proc. Natl. Acad. Sci. U. S. A.* 2020, 117 (12), 6376–6382.
- (73) Lou, Y.; Zheng, Y. P.; Li, X.; Ta, N.; Xu, J.; Nie, Y. F.; Cho, K.; Liu, J. Y. Pocketlike active site of Rh<sub>1</sub>/MoS<sub>2</sub> single-atom catalyst for selective crotonaldehyde hydrogenation. *J. Am. Chem. Soc.* **2019**, *141* (49), 19289–19295.
- (74) Yang, J.; Qiu, Z.; Zhao, C.; Wei, W.; Chen, W.; Li, Z.; Qu, Y.; Dong, J.; Luo, J.; Li, Z.; Wu, Y. In situ thermal atomization to convert supported nickel nanoparticles into surface-bound nickel single-atom catalysts. *Angew. Chem.* **2018**, *130* (43), 14291–14296.
- (75) Jones, J.; Xiong, H.; DeLaRiva, A. T.; Peterson, E. J.; Pham, H.; Challa, S. R.; Qi, G.; Oh, S.; Wiebenga, M. H.; Pereira Hernández, X. I.; Wang, Y.; Datye, A. K. Thermally stable single-atom platinum-onceria catalysts via atom trapping. *Science* **2016**, 353 (6295), 150–154.
- (76) Wei, S.; Li, A.; Liu, J.-C.; Li, Z.; Chen, W.; Gong, Y.; Zhang, Q.; Cheong, W.-C.; Wang, Y.; Zheng, L.; Xiao, H.; Chen, C.; Wang, D.; Peng, Q.; Gu, L.; Han, X.; Li, J.; Li, Y. Direct observation of noble metal nanoparticles transforming to thermally stable single atoms. *Nat. Nanotechnol.* **2018**, *13*, 856–861.
- (77) Gerber, C.; Lang, H. P. How the doors to the nanoworld were opened. *Nat. Nanotechnol.* **2006**, *1* (1), 3-5.
- (78) Higgins, S. J.; Nichols, R. J. Catalysts under the microscope. *Nat. Nanotechnol.* **2007**, 2 (5), 270–271.
- (79) Sohlberg, K.; Pennycook, T. J.; Zhou, W.; Pennycook, S. J. Insights into the physical chemistry of materials from advances in HAADF-STEM. *Phys. Chem. Chem. Phys.* **2015**, *17* (6), 3982–4006.
- (80) Bradley, S. A.; Sinkler, W.; Blom, D. A.; Bigelow, W.; Voyles, P. M.; Allard, L. F. Behavior of Pt atoms on oxide supports during reduction treatments at elevated temperatures, characterized by aberration corrected STEM imaging. *Catal. Lett.* **2012**, *142* (2), 176–182.
- (81) Pennycook, S.; Jesson, D. High-resolution Z-contrast imaging of crystals. *Ultramicroscopy* **1991**, 37 (1-4), 14-38.
- (82) Muller, D. A. Structure and bonding at the atomic scale by scanning transmission electron microscopy. *Nat. Mater.* **2009**, 8 (4), 263–270.
- (83) Liu, Q.; Zhang, Z. Platinum single-atom catalysts: a comparative review towards effective characterization. *Catal. Sci. Technol.* **2019**, 9 (18), 4821–4834.
- (84) Crewe, A. V.; Wall, J.; Langmore, J. Visibility of single atoms. *Science* **1970**, *168* (3937), 1338–1340.
- (85) Gates, B. C. Atomically dispersed supported metal catalysts: seeing is believing. *Trends in Chemistry* **2019**, *1* (1), 99–110.
- (86) He, X.; He, Q.; Deng, Y.; Peng, M.; Chen, H.; Zhang, Y.; Yao, S.; Zhang, M.; Xiao, D.; Ma, D.; Ge, B.; Ji, H. A versatile route to

- fabricate single atom catalysts with high chemoselectivity and regioselectivity in hydrogenation. Nat. Commun. 2019, 10 (1), 3663.
- (87) Bianconi, A. Surface X-ray absorption spectroscopy: Surface EXAFS and surface XANES. Appl. Surf. Sci. 1980, 6 (3-4), 392-418.
- (88) Palmer, B. J.; Pfund, D. M.; Fulton, J. L. Direct modeling of EXAFS spectra from molecular dynamics simulations. *J. Phys. Chem.* **1996**, 100 (32), 13393–13398.
- (89) Lamberti, C.; Zecchina, A.; Groppo, E.; Bordiga, S. Probing the surfaces of heterogeneous catalysts by in situ IR spectroscopy. *Chem. Soc. Rev.* **2010**, 39 (12), 4951–5001.
- (90) Chen, Y.; Huang, Z.; Ma, Z.; Chen, J.; Tang, X. Fabrication, characterization, and stability of supported single-atom catalysts. *Catal. Sci. Technol.* **2017**, 7 (19), 4250–4258.
- (91) Hoffman, A. S.; Fang, C.-Y.; Gates, B. C. Homogeneity of surface sites in supported single-site metal catalysts: assessment with band widths of metal carbonyl infrared spectra. *J. Phys. Chem. Lett.* **2016**, 7 (19), 3854–3860.
- (92) Nørskov, J. K.; Bligaard, T.; Logadottir, A.; Kitchin, J.; Chen, J. G.; Pandelov, S.; Stimming, U. Trends in the exchange current for hydrogen evolution. *J. Electrochem. Soc.* **2005**, *152* (3), J23.
- (93) Zhang, J.; Zhao, Y.; Guo, X.; Chen, C.; Dong, C.-L.; Liu, R.-S.; Han, C.-P.; Li, Y.; Gogotsi, Y.; Wang, G. Single platinum atoms immobilized on an MXene as an efficient catalyst for the hydrogen evolution reaction. *Nature Catalysis* 2018, 1 (12), 985–992.
- (94) Hunt, S. T.; Milina, M.; Wang, Z.; Román-Leshkov, Y. Activating earth-abundant electrocatalysts for efficient, low-cost hydrogen evolution/oxidation: sub-monolayer platinum coatings on titanium tungsten carbide nanoparticles. *Energy Environ. Sci.* **2016**, 9 (10), 3290–3301.
- (95) Zhang, L.; Si, R.; Liu, H.; Chen, N.; Wang, Q.; Adair, K.; Wang, Z.; Chen, J.; Song, Z.; Li, J.; Banis, M. N.; Li, R.; Sham, T.-K.; Gu, M.; Liu, L.-M.; Botton, G. A.; Sun, X. Atomic layer deposited Pt-Ru dual-metal dimers and identifying their active sites for hydrogen evolution reaction. *Nat. Commun.* 2019, 10 (1), 4936.
- (96) Zhu, C.; Shi, Q.; Xu, B. Z.; Fu, S.; Wan, G.; Yang, C.; Yao, S.; Song, J.; Zhou, H.; Du, D.; Beckman, S. P.; Su, D.; Lin, Y. Hierarchically porous M-N-C (M = Co and Fe) single-atom electrocatalysts with robust MNx active moieties enable enhanced ORR performance. Adv. Energy Mater. 2018, 8 (29), 1801956.
- (97) Wang, X. X.; Cullen, D. A.; Pan, Y.-T.; Hwang, S.; Wang, M.; Feng, Z.; Wang, J.; Engelhard, M. H.; Zhang, H.; He, Y.; Shao, Y.; Su, D.; More, K. L.; Spendelow, J. S.; Wu, G. Nitrogen-coordinated single cobalt atom catalysts for oxygen reduction in proton exchange membrane fuel cells. *Adv. Mater.* **2018**, *30* (11), 1706758.
- (98) Li, J.; Chen, M.; Cullen, D. A.; Hwang, S.; Wang, M.; Li, B.; Liu, K.; Karakalos, S.; Lucero, M.; Zhang, H.; Lei, C.; Xu, H.; Sterbinsky, G. E.; Feng, Z.; Su, D.; More, K. L.; Wang, G.; Wang, Z.; Wu, G. Atomically dispersed manganese catalysts for oxygen reduction in proton-exchange membrane fuel cells. *Nature Catalysis* 2018, 1 (12), 935–945.
- (99) Gao, G.; Jiao, Y.; Waclawik, E. R.; Du, A. Single atom (Pd/Pt) supported on graphitic carbon nitride as an efficient photocatalyst for visible-light reduction of carbon dioxide. *J. Am. Chem. Soc.* **2016**, 138 (19), 6292–6297.
- (100) Gu, J.; Hsu, C.-S.; Bai, L.; Chen, H. M.; Hu, X. Atomically dispersed Fe<sup>3+</sup> sites catalyze efficient CO<sub>2</sub> electroreduction to CO. *Science* **2019**, 364 (6445), 1091–1094.
- (101) Lin, J.; Wang, A.; Qiao, B.; Liu, X.; Yang, X.; Wang, X.; Liang, J.; Li, J.; Liu, J.; Zhang, T. Remarkable performance of Ir<sub>1</sub>/FeOx single-atom catalyst in water gas shift reaction. *J. Am. Chem. Soc.* **2013**, 135 (41), 15314–15317.
- (102) Zhu, C.; Fu, S.; Shi, Q.; Du, D.; Lin, Y. Single-atom electrocatalysts. *Angew. Chem., Int. Ed.* **2017**, *56* (45), 13944–13960. (103) Liu, J. Catalysis by supported single metal atoms. *ACS Catal.* **2017**, *7* (1), 34–59.
- (104) Guo, L.-W.; Du, P.-P.; Fu, X.-P.; Ma, C.; Zeng, J.; Si, R.; Huang, Y.-Y.; Jia, C.-J.; Zhang, Y.-W.; Yan, C.-H. Contributions of distinct gold species to catalytic reactivity for carbon monoxide oxidation. *Nat. Commun.* **2016**, 7 (1), 13481.

- (105) Rossell, M. D.; Caparrós, F. J.; Angurell, I.; Muller, G.; Llorca, J.; Seco, M.; Rossell, O. Magnetite-supported palladium single-atoms do not catalyse the hydrogenation of alkenes but small clusters do. *Catal. Sci. Technol.* **2016**, *6* (12), 4081–4085.
- (106) Yin, X.-P.; Wang, H.-J.; Tang, S.-F.; Lu, X.-L.; Shu, M.; Si, R.; Lu, T.-B. Engineering the coordination environment of single-atom platinum anchored on graphdiyne for optimizing electrocatalytic hydrogen evolution. *Angew. Chem., Int. Ed.* **2018**, *57* (30), 9382–9386.
- (107) Park, J.; Lee, S.; Kim, H.-E.; Cho, A.; Kim, S.; Ye, Y.; Han, J. W.; Lee, H.; Jang, J. H.; Lee, J. Investigation of the support effect in atomically dispersed Pt on  $WO_{3-X}$  for utilization of Pt in the hydrogen evolution reaction. *Angew. Chem., Int. Ed.* **2019**, 58 (45), 16038–16042.
- (108) Siahrostami, S.; Verdaguer-Casadevall, A.; Karamad, M.; Deiana, D.; Malacrida, P.; Wickman, B.; Escudero-Escribano, M.; Paoli, E. A.; Frydendal, R.; Hansen, T. W.; Chorkendorff, I.; Stephens, I. E. L.; Rossmeisl, J. Enabling direct H<sub>2</sub>O<sub>2</sub> production through rational electrocatalyst design. *Nat. Mater.* **2013**, *12*, 1137–1143.
- (109) Liu, M.; Wang, L.; Zhao, K.; Shi, S.; Shao, Q.; Zhang, L.; Sun, X.; Zhao, Y.; Zhang, J. Atomically dispersed metal catalysts for the oxygen reduction reaction: synthesis, characterization, reaction mechanisms and electrochemical energy applications. *Energy Environ. Sci.* 2019, 12 (10), 2890–2923.
- (110) Jung, E.; Shin, H.; Lee, B.-H.; Efremov, V.; Lee, S.; Lee, H. S.; Kim, J.; Hooch Antink, W.; Park, S.; Lee, K.-S.; Cho, S.-P.; Yoo, J. S.; Sung, Y.-E.; Hyeon, T. Atomic-level tuning of Co-N-C catalyst for high-performance electrochemical H<sub>2</sub>O<sub>2</sub> production. *Nat. Mater.* **2020**, *19*, 436–442.
- (111) Pei, G. X.; Liu, X. Y.; Yang, X.; Zhang, L.; Wang, A.; Li, L.; Wang, H.; Wang, X.; Zhang, T. Performance of Cu-Alloyed Pd single-atom catalyst for semihydrogenation of acetylene under simulated front-end conditions. ACS Catal. 2017, 7 (2), 1491–1500.
- (112) Wang, X.; Chen, Z.; Zhao, X.; Yao, T.; Chen, W.; You, R.; Zhao, C.; Wu, G.; Wang, J.; Huang, W. Regulation of coordination number over single Co sites: triggering the efficient electroreduction of CO<sub>2</sub>. Angew. Chem. **2018**, 130 (7), 1962–1966.
- (113) Cohen, A. J.; Mori-Sánchez, P.; Yang, W. Challenges for density functional theory. *Chem. Rev.* 2012, 112 (1), 289-320.
- (114) Liu, D.; Li, X.; Chen, S.; Yan, H.; Wang, C.; Wu, C.; Haleem, Y. A.; Duan, S.; Lu, J.; Ge, B.; Ajayan, P. M.; Luo, Y.; Jiang, J.; Song, L. Atomically dispersed platinum supported on curved carbon supports for efficient electrocatalytic hydrogen evolution. *Nature Energy* 2019, 4, 512–518.
- (115) Kim, H.-E.; Lee, I. H.; Cho, J.; Shin, S.; Ham, H. C.; Kim, J. Y.; Lee, H. Palladium single-atom catalysts supported on  $C@C_3N_4$  for electrochemical reactions. *ChemElectroChem* **2019**, 6 (18), 4757–4764.
- (116) Sun, M.; Wu, T.; Xue, Y.; Dougherty, A. W.; Huang, B.; Li, Y.; Yan, C.-H. Mapping of atomic catalyst on graphdiyne. *Nano Energy* **2019**, *62*, 754–763.
- (117) Lee, J.; von Gunten, U.; Kim, J.-H. Persulfate-based advanced oxidation: critical assessment of opportunities and roadblocks. *Environ. Sci. Technol.* **2020**, *54* (6), 3064–3081.
- (118) Yin, Y.; Shi, L.; Li, W.; Li, X.; Wu, H.; Ao, Z.; Tian, W.; Liu, S.; Wang, S.; Sun, H. Boosting Fenton-like reactions via single atom Fe catalysis. *Environ. Sci. Technol.* **2019**, 53 (19), 11391–11400.
- (119) Hodges, B. C.; Cates, E. L.; Kim, J.-H. Challenges and prospects of advanced oxidation water treatment processes using catalytic nanomaterials. *Nat. Nanotechnol.* **2018**, *13* (8), 642–650.
- (120) Garcia-Segura, S.; Qu, X.; Alvarez, P. J. J.; Chaplin, B. P.; Chen, W.; Crittenden, J. C.; Feng, Y.; Gao, G.; He, Z.; Hou, C.-H.; Hu, X.; Jiang, G.; Kim, J.-H.; Li, J.; Li, Q.; Ma, J.; Ma, J.; Nienhauser, A. B.; Niu, J.; Pan, B.; Quan, X.; Ronzani, F.; Villagran, D.; Waite, T. D.; Walker, W. S.; Wang, C.; Wong, M. S.; Westerhoff, P. Opportunities for nanotechnology to enhance electrochemical treatment of pollutants in potable water and industrial wastewater a perspective. *Environ. Sci.: Nano* 2020, 7 (8), 2178–2194.

- (121) Pan, M.; Wang, J.; Gao, G.; Chew, J. W. Incorporation of single cobalt active sites onto N-doped graphene for superior conductive membranes in electrochemical filtration. *J. Membr. Sci.* **2020**, *602*, 117966.
- (122) Huang, D.; Wang, K.; Niu, J.; Chu, C.; Weon, S.; Zhu, Q.; Lu, J.; Stavitski, E.; Kim, J.-H. Amorphous Pd-loaded Ti<sub>4</sub>O<sub>7</sub> electrode for direct anodic destruction of perfluorooctanoic acid. *Environ. Sci. Technol.* **2020**, *54* (17), 10954–10963.
- (123) Chen, Y.; Ji, S.; Wang, Y.; Dong, J.; Chen, W.; Li, Z.; Shen, R.; Zheng, L.; Zhuang, Z.; Wang, D. Isolated single iron atoms anchored on N-doped porous carbon as an efficient electrocatalyst for the oxygen reduction reaction. *Angew. Chem.* **2017**, *129* (24), 7041–7045.
- (124) Liu, J.; Jiao, M.; Lu, L.; Barkholtz, H. M.; Li, Y.; Wang, Y.; Jiang, L.; Wu, Z.; Liu, D.-j.; Zhuang, L. High performance platinum single atom electrocatalyst for oxygen reduction reaction. *Nat. Commun.* 2017, 8 (1), 15938.
- (125) Zhu, C.; Fu, S.; Song, J.; Shi, Q.; Su, D.; Engelhard, M. H.; Li, X.; Xiao, D.; Li, D.; Estevez, L. Self-assembled Fe—N-doped carbon nanotube aerogels with single-atom catalyst feature as high-efficiency oxygen reduction electrocatalysts. *Small* **2017**, *13* (15), 1603407.
- (126) Zhang, J.; Liu, J.; Xi, L.; Yu, Y.; Chen, N.; Sun, S.; Wang, W.; Lange, K. M.; Zhang, B. Single-atom Au/NiFe layered double hydroxide electrocatalyst: probing the origin of activity for oxygen evolution reaction. *J. Am. Chem. Soc.* **2018**, *140* (11), 3876–3879.
- (127) Deng, J.; Li, H.; Xiao, J.; Tu, Y.; Deng, D.; Yang, H.; Tian, H.; Li, J.; Ren, P.; Bao, X. Triggering the electrocatalytic hydrogen evolution activity of the inert two-dimensional MoS<sub>2</sub> surface via single-atom metal doping. *Energy Environ. Sci.* **2015**, 8 (5), 1594–1601
- (128) Zhao, Y.; Ling, T.; Chen, S.; Jin, B.; Vasileff, A.; Jiao, Y.; Song, L.; Luo, J.; Qiao, S. Z. Non-metal single-iodine-atom electrocatalysts for the hydrogen evolution reaction. *Angew. Chem., Int. Ed.* **2019**, *58* (35), 12252–12257.
- (129) Gao, C.; Low, J.; Long, R.; Kong, T.; Zhu, J.; Xiong, Y. Heterogeneous single-atom photocatalysts: fundamentals and applications. *Chem. Rev.* **2020**, DOI: 10.1021/acs.chemrev.9b00840.
- (130) Li, Y.; Wang, Z.; Xia, T.; Ju, H.; Zhang, K.; Long, R.; Xu, Q.; Wang, C.; Song, L.; Zhu, J. Implementing metal-to-ligand charge transfer in organic semiconductor for improved visible-near-infrared photocatalysis. *Adv. Mater.* **2016**, 28 (32), 6959–6965.
- (131) Tong, T.; Zhu, B.; Jiang, C.; Cheng, B.; Yu, J. Mechanistic insight into the enhanced photocatalytic activity of single-atom Pt, Pd or Au-embedded g- $C_3N_4$ . Appl. Surf. Sci. 2018, 433, 1175–1183.
- (132) Zhang, H.; Wei, J.; Dong, J.; Liu, G.; Shi, L.; An, P.; Zhao, G.; Kong, J.; Wang, X.; Meng, X. Efficient visible-light-driven carbon dioxide reduction by a single-atom implanted metal—organic framework. *Angew. Chem.* **2016**, *128* (46), 14522—14526.
- (133) Zuo, Q.; Liu, T.; Chen, C.; Ji, Y.; Gong, X.; Mai, Y.; Zhou, Y. Ultrathin metal—organic framework nanosheets with ultrahigh loading of single Pt atoms for efficient visible-light-driven photocatalytic H<sub>2</sub> evolution. *Angew. Chem.* **2019**, *131* (30), 10304–10309.
- (134) Fang, X.; Shang, Q.; Wang, Y.; Jiao, L.; Yao, T.; Li, Y.; Zhang, Q.; Luo, Y.; Jiang, H. L. Single Pt atoms confined into a metal—organic framework for efficient photocatalysis. *Adv. Mater.* **2018**, *30* (7), 1705112.
- (135) He, T.; Chen, S.; Ni, B.; Gong, Y.; Wu, Z.; Song, L.; Gu, L.; Hu, W.; Wang, X. Zirconium—porphyrin-based metal—organic framework hollow nanotubes for immobilization of noble-metal single atoms. *Angew. Chem.* **2018**, *130* (13), 3551–3556.
- (136) An, S.; Zhang, G.; Wang, T.; Zhang, W.; Li, K.; Song, C.; Miller, J. T.; Miao, S.; Wang, J.; Guo, X. High-density ultra-small clusters and single-atom Fe sites embedded in graphitic carbon nitride (g-C<sub>3</sub>N<sub>4</sub>) for highly efficient catalytic advanced oxidation processes. ACS Nano 2018, 12 (9), 9441–9450.
- (137) Wang, F.; Wang, Y.; Feng, Y.; Zeng, Y.; Xie, Z.; Zhang, Q.; Su, Y.; Chen, P.; Liu, Y.; Yao, K.; Lv, W.; Liu, G. Novel ternary photocatalyst of single atom-dispersed silver and carbon quantum dots co-loaded with ultrathin g-C<sub>3</sub>N<sub>4</sub> for broad spectrum photo-

- catalytic degradation of naproxen. Appl. Catal., B 2018, 221, 510-520.
- (138) Wang, X.; Jin, B.; Jin, Y.; Wu, T.; Ma, L.; Liang, X. Supported single Fe atoms prepared via atomic layer deposition for catalytic reactions. ACS Applied Nano Materials 2020, 3 (3), 2867–2874.
- (139) Wang, Y.; Zhao, X.; Cao, D.; Wang, Y.; Zhu, Y. Peroxymonosulfate enhanced visible light photocatalytic degradation bisphenol A by single-atom dispersed Ag mesoporous g-C<sub>3</sub>N<sub>4</sub> hybrid. *Appl. Catal., B* **2017**, *211*, 79–88.
- (140) Loeb, S. K.; Alvarez, P. J. J.; Brame, J. A.; Cates, E. L.; Choi, W.; Crittenden, J.; Dionysiou, D. D.; Li, Q. L.; Li-Puma, G.; Quan, X.; Sedlak, D. L.; Waite, T. D.; Westerhoff, P.; Kim, J. H. The technology horizon for photocatalytic water treatment: sunrise or sunset? *Environ. Sci. Technol.* 2019, 53 (6), 2937–2947.
- (141) Martin, E. T.; McGuire, C. M.; Mubarak, M. S.; Peters, D. G. Electroreductive remediation of halogenated environmental pollutants. *Chem. Rev.* **2016**, *116* (24), 15198–15234.
- (142) Qian, Y.; Guo, X.; Zhang, Y.; Peng, Y.; Sun, P.; Huang, C.; Niu, J.; Zhou, X.; Crittenden, J. C. Perfluorooctanoic acid degradation using UV-persulfate process: modeling of the degradation and chlorate formation. *Environ. Sci. Technol.* **2016**, *50* (2), 772–781.
- (143) Chaplin, B. P. Critical review of electrochemical advanced oxidation processes for water treatment applications. *Environmental Science: Processes & Impacts* **2014**, *16* (6), 1182–1203.
- (144) Baumgartner, R.; Stieger, G. K.; McNeill, K. Complete hydrodehalogenation of polyfluorinated and other polyhalogenated benzenes under mild catalytic conditions. *Environ. Sci. Technol.* **2013**, 47 (12), 6545–6553.
- (145) Doudin, N.; Yuk, S. F.; Marcinkowski, M. D.; Nguyen, M.-T.; Liu, J.-C.; Wang, Y.; Novotny, Z.; Kay, B. D.; Li, J.; Glezakou, V.-A.; Parkinson, G.; Rousseau, R.; Dohnálek, Z. Understanding heterolytic H<sub>2</sub> cleavage and water-assisted hydrogen spillover on Fe<sub>3</sub>O<sub>4</sub>(001)-supported single palladium atoms. *ACS Catal.* **2019**, 9 (9), 7876–7887.
- (146) Huang, F.; Deng, Y.; Chen, Y.; Cai, X.; Peng, M.; Jia, Z.; Ren, P.; Xiao, D.; Wen, X.; Wang, N. Atomically dispersed Pd on nanodiamond/graphene hybrid for selective hydrogenation of acetylene. J. Am. Chem. Soc. 2018, 140 (41), 13142–13146.
- (147) Vilé, G.; Albani, D.; Nachtegaal, M.; Chen, Z.; Dontsova, D.; Antonietti, M.; López, N.; Pérez-Ramírez, J. A stable single-site palladium catalyst for hydrogenations. *Angew. Chem., Int. Ed.* **2015**, *54* (38), 11265–11269.
- (148) Kyriakou, G.; Boucher, M. B.; Jewell, A. D.; Lewis, E. A.; Lawton, T. J.; Baber, A. E.; Tierney, H. L.; Flytzani-Stephanopoulos, M.; Sykes, E. C. H. Isolated metal atom geometries as a strategy for selective heterogeneous hydrogenations. *Science* **2012**, 335 (6073), 1209–1212.
- (149) Shin, H.; Jung, S.; Bae, S.; Lee, W.; Kim, H. Nitrite reduction mechanism on a Pd surface. *Environ. Sci. Technol.* **2014**, 48 (21), 12768–12774.
- (150) Yin, Y. B.; Guo, S.; Heck, K. N.; Clark, C. A.; Coonrod, C. L.; Wong, M. S. Treating water by degrading oxyanions using metallic nanostructures. *ACS Sustainable Chem. Eng.* **2018**, *6*, 11160–11175.
- (151) Temkin, A.; Evans, S.; Manidis, T.; Campbell, C.; Naidenko, O. V. Exposure-Based Assessment and Economic Valuation of Adverse Birth Outcomes and Cancer Risk Due to Nitrate in United States Drinking Water. *Environ. Res.* **2019**, *176*, 108442.
- (152) Jung, S.; Bae, S.; Lee, W. Development of Pd-Cu/hematite catalyst for selective nitrate reduction. *Environ. Sci. Technol.* **2014**, 48 (16), 9651–9658.
- (153) Darby, M. T.; Réocreux, R.; Sykes, E. C. H.; Michaelides, A.; Stamatakis, M. Elucidating the stability and reactivity of surface intermediates on single-atom alloy catalysts. *ACS Catal.* **2018**, 8 (6), 5038–5050.
- (154) Wen, H.; Huai, L.-y.; Jin, X.; Liu, J.-y. Mechanism of nitric oxide reduction by hydrogen on Ni(110) and Ir/Ni(110): first principles and microkinetic modeling. *J. Phys. Chem. C* **2019**, 123 (8), 4825–4836.

- (155) Xing, F. L.; Jeon, J.; Toyao, T.; Shimizu, K.; Furukawa, S. A Cu-Pd single-atom alloy catalyst for highly efficient NO reduction. *Chem. Sci.* **2019**, *10* (36), 8292–8298.
- (156) Asokan, C.; Yang, Y.; Dang, A.; Getsoian, A. B.; Christopher, P. Low-temperature ammonia production during NO reduction by CO is due to atomically dispersed rhodium active sites. *ACS Catal.* **2020**, *10* (9), 5217–5222.
- (157) Ding, W.-C.; Gu, X.-K.; Su, H.-Y.; Li, W.-X. Single Pd atom embedded in CeO<sub>2</sub>(111) for NO reduction with CO: a first-principles study. *J. Phys. Chem. C* **2014**, *118* (23), 12216–12223.
- (158) Beniya, A.; Higashi, S. Towards dense single-atom catalysts for future automotive applications. *Nature Catalysis* **2019**, 2 (7), 590–602
- (159) Huang, H.; Leung, D. Y. C. Complete oxidation of formaldehyde at room temperature using TiO<sub>2</sub> supported metallic Pd nanoparticles. *ACS Catal.* **2011**, *1* (4), 348–354.
- (160) Nie, L.; Yu, J.; Li, X.; Cheng, B.; Liu, G.; Jaroniec, M. Enhanced performance of NaOH-modified Pt/TiO<sub>2</sub> toward room temperature selective oxidation of formaldehyde. *Environ. Sci. Technol.* **2013**, 47 (6), 2777–2783.
- (161) Weon, S.; Choi, E.; Kim, H.; Kim, J. Y.; Park, H.-J.; Kim, S.-m.; Kim, W.; Choi, W. Active {001} facet exposed TiO<sub>2</sub> nanotubes photocatalyst filter for volatile organic compounds removal: from material development to commercial indoor air cleaner application. *Environ. Sci. Technol.* **2018**, 52 (16), 9330–9340.
- (162) He, C.; Cheng, J.; Zhang, X.; Douthwaite, M.; Pattisson, S.; Hao, Z. Recent advances in the catalytic oxidation of volatile organic compounds: a review based on pollutant sorts and sources. *Chem. Rev.* **2019**, *119* (7), 4471–4568.
- (163) Zhang, H.; Sui, S.; Zheng, X.; Cao, R.; Zhang, P. One-pot synthesis of atomically dispersed Pt on MnO2 for efficient catalytic decomposition of toluene at low temperatures. *Appl. Catal., B* **2019**, 257, 117878.
- (164) Weon, S.; He, F.; Choi, W. Status and challenges in photocatalytic nanotechnology for cleaning air polluted with volatile organic compounds: visible light utilization and catalyst deactivation. *Environ. Sci.: Nano* **2019**, *6* (11), 3185–3214.
- (165) Li, X.; Yang, X.; Zhang, J.; Huang, Y.; Liu, B. In situ/operando techniques for characterization of single-atom catalysts. *ACS Catal.* **2019**, 9 (3), 2521–2531.